EPJA manuscript No.
(will be inserted by the editor)

Equations of state for hot neutron stars - II. The role of exotic particle degrees of freedom

Adriana R. Raduta

arXiv:2205.03177v2 [nucl-th] 27 Jun 2022

Received: date / Accepted: date

Abstract Explosive astrophysical systems - such as supernovae or compact star binary mergers - provide conditions where exotic degrees of freedom can be populated. Within the covariant density functional theory of nuclear matter we build several general purpose equations of state which, in addition to the baryonic octet, account for $\Delta(1232)$ resonance states. The thermodynamic stability of Δ-admixed nuclear matter is investigated in the limiting case of vanishing temperature for charge fractions $Y_Q = 0.01$ and $Y_Q = 0.5$ and wide ranges of the coupling constants to the scalar and vector mesonic fields. General purpose equation of state models with exotica presently available on the COMPOSE database are further reviewed; for a selection of them we then investigate thermal properties for thermodynamic conditions relevant for core-collapse supernovae and binary neutron star mergers. Modifications induced by hyperons, $\Delta(1232)$, K^-, pions and quarks are discussed.

1 Introduction

In astrophysical events like core-collapse supernovae (CCSN) [1,2,3,4,5] and binary neutron star (BNS) mergers [6,7,8,9, 10,11,12] as well as in the evolution of proto-neutron stars (PNS) [13,14] and formation of stellar black holes (BH) [15, 16,17,18] high density and high temperature states of matter are populated. Under these circumstances the appearance of non-nucleonic degrees of freedom (d.o.f.) - such as hyperons, meson condensates and quarks - is highly probable. From the energetic view point these exotic phases are the natural consequence of the Pauli principle and are expected to nucleate whenever the chemical potential of neutrons exceeds a certain threshold. Limited current information on the equation of state (EoS) does nevertheless not allow to ascertain the occurrence of any of these species and even less to identify the thermodynamic conditions and astrophysical environments where one species or another will dominate over nucleonic matter.

Signatures of exotic matter are typically sought after by comparing results of numerical simulations obtained by accounting for various extra particle d.o.f. with those obtained when only nucleons are considered. As such hyperons and hadrons to quark phase transitions have been found to affect the dynamics, neutrino signals and gravitational wave (GW) emissions.

Sekiguchi et al. [19] has shown that the onset of Λ-hyperons modifies the GWs emitted by the hypermassive neutron star (HMNS) formed after BNS as well as the surrounding torus. GW were found to be modified in two respects. Firstly, the amplitude of quasiperiodic GW at the black hole formation is damped. Second, the characteristic GW frequency increases with time. According to Radice et al. [20] the production of hyperons makes waveforms louder and alter the amplitude modulation and phase evolution; other modifications concern the compactness and binding energy of the merger remnant, higher when hyperons are present. Bauswein et al. [21,22] showed that hadron-quark phase transitions occurring during the post-merger phase modify the relation between the frequency of dominant gravitational-waves and the tidal deformability during the inspiral. Patterns of inspiral and postmerger GW signals have been confronted by Most et al. [23], who shown that the latter has the potential to bare clear signatures of phase transitions. Weith et al. [24] demonstrated that the postmerger GW signal exhibits two distinct fundamental frequencies before and after the phase transition. More precisely, if the collapse into a BH is triggered by the phase transition, the frequencies

Adriana R. Raduta
National Institute for Physics and Nuclear Engineering (IFIN-HH), RO-077125 Bucharest, Romania
E-mail: araduta@nipne.ro

of GW emitted by the HMHS increase as the collapse proceeds; if, at variance, the phase transition develops after the merger and a metastable object with a quark-matter core is formed, the transition to a signal at higher frequencies is more smooth and the largest values are smaller than in the first scenario. Modification of post-merger GW frequencies by the quark deconfinement phase transition is confirmed also by Prakash et al. [11] who have additionally studied modifications of dynamical ejecta, remnant accretion disk masses, *r*-process nucleosynthesis yields and electromagnetic counterparts.

Effects of pions, hyperons and hadron-quark phase transition in stellar core collapse have been identified as well. According to Sagert et al. [25], phase transitions occurring during the early postbounce evolution might produce a second shock wave. If this is strong enough a delayed supernova explosion is triggered and an additional neutrino-peak generated. Zha et al. [26] have proved that if, due to the QCD phase transition, the PNS collapses following the core-collapse, a loud burst of GW is formed. Its properties - amplitude, frequency range, duration, energy - are different than those of normally found postbounce GW. According to Lin et al. [27] the neutrino signal emitted by these failed CCSN is oscillatory. Effects of pions and Λ-hyperons, including a possible strangeness-driven phase transition on the evolution of core collapse and formation of stellar BH have been considered in Peres et al. [28]. It was found that the EoS softening results in reduced (increased) values of central density (temperature) at bounce; increased radii of the homologous core and PNS; steeper increase of central density during postbounce; faster collapse into BH. The magnitude of modifications increases with abundances of exotic species. Phase transitions additionally induce core oscillations.

The consequences of phase transitions, non-monotonic density-dependence of the sound speed and numerical accidents in the surface of thermodynamic potentials have been discussed by Aloy et al. [29]. Among their results we remind the supersonic behavior of the infalling matter in connection with a phase transition.

Numerical simulations of these phenomena require detailed information on composition, thermodynamic and, preferably also, microscopic properties of matter over wide domains of baryonic density 10^{-14} fm$^{-3} \leq n_B \leq 1.5$ fm^{-3}, electron fraction $0 \leq Y_e = n_e/n_B \leq 0.6$ and temperature $0 \leq T \leq 100$ MeV. The first so-called general purpose EoS tables for astrophysical use have been made available by Lattimer and Swesty [30] and Shen et al. [31,32] and accounted only for nucleonic d.o.f. For almost two decades they were the only ones to exist. As such more "finite-temperature" EoS have been built heuristically by the so-called Γ-law, which consists in supplementing cold EoS with ideal-gas thermal contributions - a method still in use, see Sec. 6. Starting with 2010 the situation improved significantly and today almost one hundred such EoS exist. Out of them 36 account also for one or several exotic particles. These EoS tables have been obtained within different theoretical frameworks; rely on various baryon-baryon interactions; implement different constraints derived from nuclear physics, astrophysics and *ab initio* calculations; for a review, see [33, 34]. Though the collection of existing models is still far from exhausting the huge parameter space associated with the uncertainties in effective baryonic interactions at high densities and isospin asymmetries, it allowed to identify how particle abundances depend on thermodynamic conditions; the extend in which exotic d.o.f. impact on thermodynamic state variables or derived quantities like adiabatic index or speed of sound; whether correlations exist with EoS of nuclear matter; investigate properties of isentropic PNS and the relation with their nucleonic counterparts [35,28,36,37,38,39, 40,41].

The first aim of this work is to present three general purpose EoS models that account for the baryonic octet and $\Delta(1232)$-resonances. They are derived in the framework of the covariant density functional theory (CDFT), are available on the CompOSE site [1] [42,43] and - to our knowledge - are the first publicly available EoS models which account for Δs. Accounting for Δs, in principle, one may face first order phase transition(s) in thermodynamic conditions relevant for astrophysics [44]. Our EoS models are built by giving to the coupling constants to meson fields values in accord with present constraints. When the contribution of the neutralizing electron gas is accounted for none of these models manifests instabilities. Though, when only baryonic matter is considered, one of the models shows Δ-driven instabilities.

The second motivation is to provide a better understanding of the finite-T behavior of EoS models with exotic d.o.f. To this end we review general purpose EoS tables with exotica presently available on the CompOSE site. Then, for a collection of EoS models which allow for different exotic d.o.f. and have the property that general purpose EoS tables for purely nucleonic matter exist as well a comparative study is performed for a series of thermal properties. These two aspects make present work be the follow-up of our previous paper devoted to EoS with nucleonic d.o.f. [45], called in the following Paper I.

The paper in organized as follows. General purpose EoS with exotica presently available on the CompOSE site are reviewed in Sec. 2. Sec. 3 offers an overview of CDFT models with density-dependent couplings. The role of hyperons and Δ-resonances at finite-T is analyzed in Sec. 5 by considering simplified mixtures of nucleons and the Λ-hyperons and, respectively, Δs. Thermodynamic stability of cold Δ-admixed nucleonic matter at $T = 0$ is investigated in Sec. 5. Thermal properties of a large collection of models, including

[1] https://compose.obspm.fr/

the newly proposed ones, are addressed in Sec. 6. In order to better highlight the role of various particle d.o.f. or the way in which the hadron to quark phase transition is implemented none of the currently used constraints on parameters of nuclear matter at saturation or properties of NS is used as a filter.

Throughout this paper we use the natural units with $c = \hbar = k_B = G = 1$.

2 General purpose EoS models with exotic particle degrees of freedom on COMPOSE

In this section we provide an overview of models with exotic particle degrees of freedom for which general purpose EoS tables are available on the COMPOSE site. General purpose tables cover large ranges of baryon number densities n_B, temperatures T, and electron fractions Y_e and are ready to use in numerical simulations of CCSN, PNS and BNS mergers. Contributions of electron-positron and photon gases, treated as ideal Fermi and Bose gases, are included in all tables assuming that the net electron fraction equals the baryon charge fraction, $Y_e = Y_Q$, and that the different sectors are in thermal equilibrium. For some models tables corresponding to pure baryonic matter are also provided.

The standard format for the name of a particular EoS table takes the form XXX(YYY)zzz. XXX thereby indicates the initials of the authors in the original publication(s) proposing the corresponding model. YYY represents the name of the interaction and provides information on the effective nucleon potential and non-nucleonic particle degrees of freedom. zzz offers extra information on coupling constants in the exotic sector, if tables are provided for more than one XXX(YYY) model.

Table 1 lists the presently available tables, along with information on the exotic particles and properties of corresponding cold β-equilibrated NS. With the exception of GROM(LS220L), which relies on a non-relativistic Skyrme-like effective interaction, all the models belong to CDFT. The nuclear matter (NM) parameters of underlying nucleonic effective interactions are provided in Table 2. As with the exception of DNS(CMF) [74,75] and BBKF(DD2F-SF) [76, 21,77] COMPOSE provides also general purpose EoS for purely nucleonic matter and these have been discussed at length in Paper I here we shall focus only on exotic d.o.f. and the supra-saturation regime.

Experimental challenges due to the short lifetime of hyperons as well as low intensity beams make that only a few hundreds scattering events exist for $N\Lambda$ and $N\Sigma$; only a few scattering events exist for $N\Xi$; no scattering data is available for YY. Unsufficient constraints on the hyperon-nucleon potentials are reflected in different predictions of various models in spite of accurate description of scattering phase shifts [82,83,84]. Realistic two-body baryon–baryon interactions that describe the scattering data in free space along with phenomenological three body forces have been exploited in microscopic approaches in order to extract the EoS of hyperon admixed NS matter. Brueckner-Hartree-Fock calculations of hypernuclear matter in [85,86,87,88] proved to be unable to produce maximum NS mass of $\approx 2M_\odot$, which was in part explained by a three body interaction not repulsive enough; for more, see [34].

An alternative solution to extract information on the YN and YY interactions relies on the study of hypernuclei, bound systems composed of nucleons and one or more hyperons. So far more than 40 single-Λ nuclei and a few double-Λ and single-Ξ nuclei have been produced and studied. The first estimation of the well depth of the Λ-hyperon in nuclear matter, $U_\Lambda^{(N)}(n_{sat}) \approx -30$ MeV, has been obtained from the extrapolation at $A \to \infty$, where A is the hypernucleus mass number, of the experimental binding energy of single-Λ hypernuclei [89]. Calibration of $\sigma\Lambda$ and $\omega\Lambda$ vertices on experimental data of binding energies of nuclei with a variable number of nucleons and one Λ, realized by solving the Dirac equations of the nucleons and the hyperon, confirm this value [90]. [90] also shows that $U_\Lambda^{(N)}$ is little affected by the assumed nucleonic effective interaction and flavor symmetry arguments used for the vector mesons. The method in [90] was further employed in [91] to calibrate the coupling constants of the Ξ-hyperon to the experimental binding energy of the single-Ξ nuclei ${}^{15}_{\Xi^-}$C and ${}^{12}_{\Xi^-}$Be. The thus obtained values -18.8 MeV $\lesssim U_\Xi^{(N)}(n_{sat}) \lesssim -14.6$ MeV, which depend on the nucleon effective interaction, are in fair agreement with the value deduced from inclusive (K^-, K^+) spectra, $U_\Xi^{(N)}(n_{sat}) \approx -15$ MeV [92] and underestimate the more attractive $U_\Xi^{(N)}(n_{sat}) \lesssim -20$ MeV obtained from $\Xi^- p \to \Lambda\Lambda$ two body capture events in ^{12}C and ^{14}N [93]. Experimental data on strong-interaction level shifts, widths and yields collected from Σ^- atoms and inclusive (π^-, K^+) spectra on medium to heavy targets indicate a repulsive but loosely constrained ΣN potential $U_\Sigma^{(N)}(n_{sat}) \approx 30 \pm 20$ MeV [89, 92].

$-U_\Lambda^{(\Lambda)}(n_{sat})$ is extracted by identification with the $\Lambda\Lambda$ bond energy, $\Delta B_{\Lambda\Lambda} = B_{\Lambda\Lambda}\left({}^{A}_{\Lambda\Lambda}Z\right) - 2B_\Lambda\left({}^{A-1}_{\Lambda}Z\right)$, where $B\left({}^{A}Z\right)$ stays for the binding energy of the nucleus ${}^{A}Z$, in double Λ hypernuclei. The initial value, $\Delta B_{\Lambda\Lambda} = 1.01 \pm 0.2^{+0.18}_{-0.11}$ MeV obtained in the KEK event [94] was revised to 0.67 ± 0.17 MeV [95] due to a change in the value of the Ξ^- mass. The small value of this attractive potential makes it that it is overlooked in most EoS model calculations.

For EoS models which account for hyperons, Table 3 lists the values of well depths in symmetric saturated matter on which the coupling constant to the σ meson has been fixed, the meson couplings and the flavor symmetry group assumed for deciding the strengths of vector mesons. One

Table 1 List of general purpose EoS tables with exotic degrees of freedom, available on COMPOSE. For each EoS model we provide information on: considered degrees of freedom; maximum mass of cold β-equilibrated NS (M_G^{max}); radius of canonical $1.4M_\odot$ NS (R_{14}); radius of a $2.072M_\odot$ NS ($R_{2.072}$); limits of combined tidal deformability $\tilde{\Lambda} = 16\left[(M_1+12M_2)M_1^4\Lambda_1+(M_2+12M_1)M_2^4\Lambda_2\right]/13\,(M_1+M_2)^5$ corresponding to the GW170817 event with an estimated total mass $M_T = 2.73^{+0.04}_{-0.01}M_\odot$ and a mass ratio range $0.73 \leq q = M_2/M_1 \leq 1$. Present astrophysical constraints on EoS regard: i) the lower limit of maximum gravitational mass [46,47,48,49,50]; ii) radii of canonical mass NS [51,52]; iii) radii of a massive NS [53,54]; iv) range for the tidal deformability obtained from the GW170817 event [55,56,57]. As in Paper I models in tension with constraint i) $M \geq 2.01-0.04M_\odot$ [47] are marked in bold. Values outside the ranges ii) $11.80 \leq R(1.4M_\odot) \leq 13.10$ km [53], iii) 11.41 km $\leq R(2.072M_\odot) \leq 13.69$ km [54], iv) $110 \leq \tilde{\Lambda} \leq 800$ [57] are also marked in bold. For M_G^{max} and R_{14} provided are the values on COMPOSE or the original publications. As in Paper I $R_{2.072}$, $\tilde{\Lambda}(q=0.73)$ and $\tilde{\Lambda}(q=1)$ are calculated by using for the crust the EoS models by [58] and [59]. n.a. (not available) means that quantities could not be calculated from the table, the reason being that, for baryonic densities exceeding a certain value, Y_e of β-equilibrated matter is lower than the lowest value in the table. Other notations are: q stands for u, d, s quarks; Λ denotes the Λ-hyperon; Δ is the $\Delta(1232)$ resonance; Y generically denotes the Λ, Σ and Ξ hyperons; π and K respectively stand for pions and kaons.

model	non-nucleonic d.o.f	M_G^{max} ($M_\odot$)	R_{14} (km)	$R_{2.072}$ (km)	$\tilde{\Lambda}$ q=0.73	$\tilde{\Lambda}$ q=1	Ref.
GROM(LS220L) no low densities	Λ	**1.91**	12.4	-	576	498	[30,35]
GROM(LS220L) with low densities	Λ	**1.91**	12.4	-	576	498	[30,35]
STOS(TM1L)	Λ	**1.90**	**14.4**	-	**1366**	**1283**	[31,32,60]
IOTSY(TM1Y-30)	Y	**1.63**	**14.3**	-	-	**1258**	[61]
IOTSY(TM1Y0)	Y	**1.64**	**14.3**	-	**1361**	**1286**	[61]
IOTSY(TM1Y30)	Y	**1.64**	**14.3**	-	**1362**	**1286**	[61]
IOTSY(TM1Y90)	Y	**1.64**	**14.3**	-	**1362**	**1286**	[61]
IOTSY(TM1Ypi-30)	Y,π	**1.66**	**13.6**	-	**844**	781	[61]
IOTSY(TM1Ypi0)	Y,π	**1.66**	**13.6**	-	**858**	778	[61]
IOTSY(TM1Ypi30)	Y,π	**1.66**	**13.6**	-	**858**	778	[61]
IOTSY(TM1Ypi90)	Y,π	**1.66**	**13.6**	-	**858**	778	[61]
SFHPST(TM1B139)	q	2.08	12.6	-	n.a.	n.a.	[31,32,25,62,63]
SFHPST(TM1B145)	q	2.01	13.0	-	n.a.	n.a.	[31,32,25,62,63]
SFHPST(TM1B155)	q	**1.70**	**10.7**	-	n.a.	n.a.	[31,32,25,62,63]
SFHPST(TM1B165)	q	**1.51**	**9.1**	-	n.a.	n.a.	[31,32,25,62,63]
FOP(SFHoY)	Y	1.99	11.9	-	401	366	[64,65,66]
BHB(DD2L)	Λ	**1.95**	**13.2**	-	787	757	[64,67]
BHB(DD2Lphi)	Λ	2.10	**13.2**	12.2	790	757	[64,67]
OMHN(DD2Y)	Y	2.03	**13.2**	-	787	756	[64,68]
MBB(DD2K)	K^-	2.19	**13.2**	13.0	798	758	[64,69]
MBB(BHBLphiK)	Λ, K^-	2.05	**13.2**	-	788	755	[64,70]
SDGTT(QMC-A)	Y	2.08	13.0	n.a.	n.a.	n.a.	[71,72,73]
R(DD2YDelta)(1.1;1.1;1.0)	YΔ	2.04	12.97	-	697	643	[64], this work
R(DD2YDelta)(1.2;1.1;1.0)	YΔ	2.05	12.30	-	470	434	[64], this work
R(DD2YDelta)(1.2;1.3;1.0)	YΔ	2.03	**13.25**	-	786	757	[64], this work
DNS(CMF)	Y, q	2.1	**14.0**	12.6	**1114**	**1043**	[74,75]
BBKF(DD2F-SF)1.1	q	2.13	12.2	**10.7**	507	467	[76,21,77]
BBKF(DD2F-SF)1.2	q	2.15	12.2	11.4	501	473	[76,21,77]
BBKF(DD2F-SF)1.3	q	2.02	12.2	-	512	467	[76,21,77]
BBKF(DD2F-SF)1.4	q	2.02	12.2	-	516	467	[76,21,77]
BBKF(DD2F-SF)1.5	q	2.03	12.2	-	488	467	[76,21,77]
BBKF(DD2F-SF)1.6	q	2.00	12.2	-	513	467	[76,21,77]
BBKF(DD2F-SF)1.7	q	2.11	12.2	**11.2**	514	467	[76,77]
BBKF(DD2-SF)1.8	q	2.06	**11.0**	-	218	180	[76,77]
BBKF(DD2-SF)1.9	q	2.17	**11.3**	**11.2**	228	196	[76,77]

can see that all models are in fair agreement or marginally consistent with present constraints on $U_\Lambda^{(N)}$ and $U_\Xi^{(N)}$. The wide range explored by $U_\Sigma^{(N)}$ allows one to inspect the consequences entailed by uncertainties in the $N\Sigma$ interaction. So far this aspect was systematically addressed only for cold β-equilibrated NS [91,96]. Out of the considered models only IOTSY models [61] account for YY potentials. The assumed values are: $U_\Sigma^{(\Sigma)} \approx U_\Lambda^{(\Sigma)} \approx U_\Sigma^{(\Lambda)} \approx 2U_\Lambda^{(\Lambda)} \approx -40$ MeV.

Some of IOTSY models [61] also account for free thermal pions. Modification of pion masses due to the interaction is disregarded. $\pi^{-,0,+}$ number densities account for s-wave pion condensation. This holds when the absolute value of pion chemical potentials equals the pion mass. Pion chemical potentials are calculated as $\mu_{\pi^+} = \mu_Q$, $\mu_{\pi^0} = 0$, $\mu_{\pi^-} = -\mu_Q$, where $\mu_Q = \mu_p - \mu_n$ is the charge chemical potential.

MBB(DD2K) [69] accounts for thermal (anti)kaons and a Bose–Einstein condensate of K^- mesons. The phase transition from the nuclear to antikaon condensed phase is second-order. Nucleons in the antikaon condensed phase behave differently than those in the hadronic phase. Kaon-nucleon in-

Table 2 List of nucleonic effective interactions on which general purpose EoS tables in Table 1 are built. For each interaction we specify the properties of symmetric nuclear matter at saturation density (n_{sat}): energy per nucleon (E_{sat}); compression modulus (K_{sat}); skewness (Q_{sat}); symmetry energy (J_{sym}); slope (L_{sym}); curvature (K_{sym}) and skewness (Q_{sym}) of the symmetry energy.

int.	n_{sat} (fm^{-3})	E_{sat} (MeV)	K_{sat} (MeV)	Q_{sat} (MeV)	J_{sym} (MeV)	L_{sym} (MeV)	K_{sym} (MeV)	Q_{sym} (MeV)	Ref.
LS220	0.155	-16.64	219.85	-410.80	28.61	73.81	-24.04	96.17	[30]
TM1	0.145	-16.26	281.16	-285.22	36.89	110.79	33.63	-66.54	[78]
SFHo	0.158	-16.19	245.4	-467.8	31.57	47.10	-205.5	n.a.	[65]
DD2	0.149	-16.02	242.72	168.65	31.67	55.04	-93.23	598.14	[79]
DD2F	0.149	-16.02	242.72	168.65	31.67	55.04	-93.23	598.14	[80]
CMF	0.15	-16.0	300	281	30	88	27	n.a.	[81,74]
QMC-A	0.156	-16.2	292	n.a.	28.5	54.0	n.a.	n.a.	[73]

Table 3 Details on CDFT models on which EoS tables have been built: list of meson couplings and/or their type (col. 6); list of hidden-strangeness mesons (if any) (col. 7); quark flavor symmetry group on which vertices of vector mesons to exotica have been fixed (col. 8). DD stays for density-dependent. For FOP(SFHoY) $i = 1,...,6$; $j = 1,...,3$. $U_X^{(N)}(n_{sat})$, eq. (24), stays for the well depth of the particle X at rest in symmetric saturated nuclear matter.

model	$U_\Lambda^{(N)}(n_{sat})$ [MeV]	$U_\Sigma^{(N)}(n_{sat})$ [MeV]	$U_\Xi^{(N)}(n_{sat})$ [MeV]	$U_\Delta^{(N)}(n_{sat})$ [MeV]	meson couplings	hidden str. mesons	flavor sym.	Ref.
STOS(TM1L)	-30	-	-	-	σ^3, σ^4, ω^4	-	SU(6)	[60]
IOTSY(TM1Y-30)	-30	-30	-15	-	σ^3, σ^4, ω^4	σ^*, ϕ	SU(3)	[61]
IOTSY(TM1Y0)	-30	0	-15	-	σ^3, σ^4, ω^4	σ^*, ϕ	SU(3)	[61]
IOTSY(TM1Y30)	-30	30	-15	-	σ^3, σ^4, ω^4	σ^*, ϕ	SU(3)	[61]
IOTSY(TM1Y90)	-30	90	-15	-	σ^3, σ^4, ω^4	σ^*, ϕ	SU(3)	[61]
IOTSY(TM1Ypi-30)	-30	-30	-15	-	σ^3, σ^4, ω^4	σ^*, ϕ	SU(3)	[61]
IOTSY(TM1Ypi0)	-30	0	-15	-	σ^3, σ^4, ω^4	σ^*, ϕ	SU(3)	[61]
IOTSY(TM1Ypi30)	-30	30	-15	-	σ^3, σ^4, ω^4	σ^*, ϕ	SU(3)	[61]
IOTSY(TM1Ypi90)	-30	90	-15	-	σ^3, σ^4, ω^4	σ^*, ϕ	SU(3)	[61]
FOP(SFHoY)	-30	30	-14	-	σ^3, σ^4, ω^4, $\sigma^i\rho^2$, $\omega^{2j}\rho^2$	ϕ	SU(6)	[66]
BHB(DD2L)	-30	-	-	-	DD	-	SU(6)	[67]
BHB(DD2Lphi)	-30	-	-	-	DD	ϕ	SU(6)	[67]
OMHN(DD2Y)	-30	30	-18	-	DD	σ^*, ϕ	SU(6)	[68]
SDGTT(QMC-A)	-28	-0.96	-12.7	-	QMC	-	-	[73]
R(DD2YDelta)(1.1;1.1;1.0)	-28	30	-20	-83	DD	ϕ	SU(6)	this work
R(DD2YDelta)(1.2;1.1;1.0)	-28	30	-20	-124	DD	ϕ	SU(6)	this work
R(DD2YDelta)(1.2;1.3;1.0)	-28	30	-20	-57	DD	ϕ	SU(6)	this work
DNS(CMF)	-28	5	-18	-	σ^4, δ^4, ω^4, $\sigma^2\delta^2$	σ^*, ϕ	SU(3)	[75]

teraction is considered in the same footing as the nucleon–nucleon interaction. Kaon-vector meson coupling constants are fixed by flavor symmetry arguments. The scalar coupling constant is determined from the real part of K^- optical potential at the saturation density, $U_{K^-}^{(N)} = -120$ MeV. MBB(BHBLphiK) [70] additionally accounts for Λ-hyperons.

BBKF(DD2-SF) and BBKF(DD2F-SF) models [77] rely on a two-phase approach for quark-hadron phase transitions, which leads by construction to a first-order phase transition. In the hadron sector only nucleonic d.o.f. are considered; in the quark sector only up and down quarks are allowed. The quark confinement is modeled within the string-flip model [76]. The fact that hadrons are composite particles made of quarks is not considered in this description. As frequently done in astrophysics, each phase is derived independently and the two phases are then merged through a mixed phase construction. The solution adopted in this work assumes thermal, mechanical and baryonic chemical equilibrium between pure hadron and quark phases. The equality of charge chemical potentials between coexisting phases is replaced, for convenience, by the equality of charge fractions. It is argued that this simplification has only little effect on thermodynamics due to the close values of charge fraction in the coexisting phases, which is a peculiarity of this model. The neutralizing electron gas is added after the phase construction is realized, which means that it does not affect phase coexistence. Throughout this work we shall refer to this phase-construction as approximate Gibbs construction; the attribute "approximate" is a reminder that the equality of charge chemical potentials is not exactly fulfilled, as it should be in the case of a Gibbs construction. We remind that the Gibbs construction is the generalization of Maxwell construction for systems with more than one conserved charge. The quark model is much more affected by temperature than the hadron model, which can be explained

by the lower masses of quarks. With rising temperature the model features a monotonic decrease of transition pressure and (baryon) chemical potential. For more, see Sec. 6.

In the hadronic-quark SFHPST-models [25,62] the hadronic sector is treated within CDFT while for the quark sector the MIT bag model is employed. In the hadron sector only nucleonic d.o.f. are considered; up, down and strange quarks are considered in the quark sector. The onset of the hadron-quark phase transition and the width of the phase coexistence domain are governed by the model parameters, i.e. strange quark mass, bag constant and strong coupling constant. By increasing the temperature the phase coexistence domain shifts to lower densities without significant modification of width. The phase transition is implemented based on a Glendenning construction [97]. At variance with the Gibbs construction which implies thermal, mechanical and chemical equilibrium of all conserved charges calculated at the boundaries of the coexistence phase here the equilibrium is imposed between different phases in the phase coexistence domain. As a consequence the pressure does no longer stay constant in the mixed phase but varies continuously with the proportion of phases in equilibrium; the conserved charges can be shared in different concentrations in each phase; the energy density is not a linear function of the proportion of phases. Moreover charge neutrality is not assumed to hold for each of the coexisting phases but for their mixture. The advantage of the Glendenning construction over the Gibbs one consists in that external fields sensitive to density, as the gravitational field, will not separate the phases [97]. Characteristic features of SFHPST-models, different from those of BBKF-models, will be discussed in Sec. 6.

The SU(3) Chiral Mean Field (CMF) model [75] is another example of EoS model which allows for hadrons and quarks. For the hadronic phase, which accounts for the whole baryonic octet, a non-linear realization of the SU(3) sigma model with an explicit chiral symmetry breaking term is used. The particle d.o.f. populated under various thermodynamic conditions change from hadrons to quarks and vice-versa through the introduction of an extra field Φ in the effective masses of baryons and quarks. Hadrons are included as quasi-particle d.o.f. in a chemically equilibrated mixture with quarks, which results in full miscibility of hadrons and quarks.

The microscopic SDGTT(QMC-A) model [73] is based on the effective relativistic mean field quark-meson-coupling (QMC) model [72]. At variance with CDFT models, in QMC the interaction between baryons takes place self-consistently between valence quarks, confined in non-overlapping baryons. The effect of the dense medium surrounding the baryons is modeled by the dynamics of quarks inside the individual particles. The parameters of the quark bag model, representing baryons, are adjusted to reproduce the masses of the baryon octet in free space. The meson fields are coupled to the quarks.

The three R(DD2YDelta)-models in Table 1 are proposed in this paper and are the first publicly available general purpose EoS models accounting for the baryonic octet and Δ-resonances. These EoS tables have been obtained in the framework of CDFT assuming that Δs preserve their vacuum masses and have vanishing widths. The numbers in parenthesis correspond to the coupling constants of the Δ to σ, ω and ρ-mesonic fields, expressed as ratios with respect to couplings of nucleons. These values span a certain range in the parameter space associated to the nucleon-Δ interaction; for a discussion on present constraints, see Sec. 5. For the inhomogeneous matter at sub-saturation densities the HS(DD2) data on CompOSE are used. They have been obtained in the framework of the extended Nuclear Statistical Equilibrium (NSE) model by Hempel and Schaffner-Bielich [64]. The transition from inhomogeneous to homogeneous matter is done for fixed values of T and Y_Q by minimizing the free energy. Data in Table 1 show that models R(DD2YDelta)(1.1;1.1;1.0) and R(DD2YDelta)(1.2;1.1;1.0) are consistent with available constraints from observation of compact stars, specifically, massive NS; radii and masses inferences by NICER; range of tidal deformability derived from GW170817. R(DD2YDelta)(1.2;1 has a more modest performance when confronted with astrophysics data as it provides for R_{14} a value exceeding the maximum value extracted from observations on PSR J0030+0451 [51,52]. Compliance with constraints from nuclear physics experiments and ab initio calculations of nuclear matter is warranted by the use of DD2 effective interaction [98]; compliance with hyper-nuclear physics data is met by the values of $U_Y^{(N)}$ on which meson coupling constants have been tuned. Also available are tables for purely baryonic matter. The domains of temperature, baryonic number density and charge fraction covered by these EoS tables and the corresponding numbers of mash points are provided in Table 4 in the Appendix A. The table corresponding to $(1.2, 1.1, 1.0)$ is unique in the sense that pure baryonic matter manifests a small Δ-driven instability domain, see Sec. 5. This instabilities are suppressed by the electron gas, which means that numerical simulations of astrophysics phenomena should not present signals typically associated with phase transitions. Provided that the values of coupling constants comply with experimental constraints, this collection of models can be extended such as to include also models that present instabilities.

3 Covariant density functional models for baryonic matter

Covariant density functional or, equivalently, relativistic mean field (RMF) models have been successfully used to describe

infinite nuclear matter, finite nuclei and stellar matter. They rely on the Walecka model [99], which treats nucleons as fundamental particle d. o. f. that interact with each other through the exchange of scalar and vector mesons. The scalar isoscalar σ and vector isoscalar ω fields correspond to these mesons and account for the attractive and repulsive parts of the nuclear interaction.

With the aim of better describing an ever increasing amount of data the original model was further developed by accounting for other mesons, e.g. the vector-isovector ρ, scalar-isovector δ and, if strange baryons are considered, also hidden-strangeness scalar-isoscalar σ^* and vector-isoscalar ϕ mesons. Models with mixed interaction terms and density dependent coupling constants have been proposed as well. For a review, see [100].

As the data generated for this paper and discussed in Sec. 4, 5 and partially 6, have been obtained in the framework of density dependent models in the following we shall review equations pertaining to this class of models. For the sake of brevity we shall limit ourselves to σ, ω, ρ, ϕ mesonic fields. These are the only mesons considered in Sec. 4, 5 as well as the new general purpose EoS with hyperons and Δs that we present here and made available on the CompOSE database. We nevertheless mention that density dependent RMF models which account for δ and/or σ^* mesons exist as well. Examples in this sense are offered by [101,102] and [90, 41] for the scalar-isovector δ and hidden-strangeness scalar-isoscalar σ^* mesons, respectively. The scalar-isovector δ meson gives rise to attraction in the isovector channel, while the vector-isovector ρ meson is responsible for repulsion; improves the neutron-proton effective mass splitting with respect to predictions of relativistic Brueckner Hartree-Fock calculations. The hidden-strangeness scalar-isoscalar σ^* meson regulates, together with the vector-isoscalar ϕ meson, the YY interaction. The scalar-isovector δ meson mostly affects the high-density behavior of the EoS while the scalar σ^* field is dominant at low densities. The role of the δ-meson in stellar matter was addressed in [103], where different hadronic contents, temperature profiles and lepton fractions have been considered. According to these authors, who employed a non-linear RMF model, inclusion of δ makes the EoS of cold and β-equilibrated nucleonic matter stiffer while the opposite effect is obtained for hyperonic matter; smaller modifications are obtained for protoneutron stars with trapped neutrinos. We expect RMF models with density dependent couplings to agree with above cited results only for cold and β-equilibrated matter.

At finite temperature, T, the scalar and number densities of a baryon i are given by

$$n_i^s = \frac{2J_i+1}{2\pi^2}\int_o^\infty \frac{k^2 m_i^*}{E_i(k)}\left[f_{\rm FD}(E_i(k)-\mu_i^*)+f_{\rm FD}(E_i(k)+\mu_i^*)\right]dk\ , \tag{1}$$

$$n_i = \frac{2J_i+1}{2\pi^2}\int_o^\infty k^2\left[f_{\rm FD}(E_i(k)-\mu_i^*)-f_{\rm FD}(E_i(k)+\mu_i^*)\right]dk\ , \tag{2}$$

where k, $E_i(k)=\sqrt{k^2+m_i^{*,2}}$, m_i^* and μ_i^* respectively stand for the wave number, kinetic part of the single particle energy, Dirac effective mass and effective chemical potential and $f_{FD}(\varepsilon)=1/\left[1+\exp(\varepsilon/T)\right]$ represents the Fermi-Dirac distribution function; $(2J_i+1)$ represents the spin degeneracy factor of the i baryon. Dirac effective mass and effective chemical potential are linked to bare mass and chemical potential by

$$m_i^* = m_i + \Sigma_{S;i}\ , \tag{3}$$

$$\mu_i^* = \mu_i - \Sigma_{V;i} - \Sigma_R\ . \tag{4}$$

with the scalar $\Sigma_{S;i}$ and vector $\Sigma_{V;i}$ self-energies and rearrangement term Σ_R expressed by

$$\Sigma_{S;i} = -g_{\sigma i}\bar{\sigma}\ , \tag{5}$$

$$\Sigma_{V;i} = g_{\omega i}\bar{\omega}+g_{\rho i}t_{3i}\bar{\rho}+g_{\phi i}\bar{\phi}\ , \tag{6}$$

$$\Sigma_R = \sum_j\left(\frac{\partial g_{\omega j}}{\partial n_j}\bar{\omega}n_j+t_{3j}\frac{\partial g_{\rho j}}{\partial n_j}\bar{\rho}n_j+\frac{\partial g_{\phi j}}{\partial n_j}\bar{\phi}n_j-\frac{\partial g_{\sigma j}}{\partial n_j}\bar{\sigma}n_j^s\right)\ . \tag{7}$$

t_{3i} represents the third component of isospin of baryon i with the convention that $t_{3p}=1/2$. As non-linear interaction terms are disregarded, the mean-field expectation values of meson fields are given by

$$m_\sigma^2\bar{\sigma} = \sum_i g_{\sigma i}n_i^s, \tag{8a}$$

$$m_\omega^2\bar{\omega} = \sum_i g_{\omega i}n_i, \tag{8b}$$

$$m_\phi^2\bar{\phi} = \sum_i g_{\phi i}n_i, \tag{8c}$$

$$m_\rho^2\bar{\rho} = \sum_i g_{\rho i}t_{3i}n_i, \tag{8d}$$

where m_m with $m=\sigma,\omega,\rho,\phi$, stays for the meson masses.

Baryonic energy density and pressure can be cast as sums between a kinetic and an interaction term,

$$e_{baryon} = e_{kin}+e_{meson}\ , \tag{9}$$

$$p_{baryon} = p_{kin}+p_{meson}+p_{rearrang}\ . \tag{10}$$

In eq. (10) an additional "rearrangement" term exists,

$$p_{rearrang} = n_B\Sigma_R\ , \tag{11}$$

due to the couplings' density-dependence.

The kinetic terms in eqs. (9) and (10) account for kinetic contributions of every species,

$$e_{kin} = \sum_i \frac{2J_i+1}{2\pi^2}\int_0^\infty dk k^2 E_i(k) \cdot \left[f_{FD}\left(E_i(k)-\mu_i^*\right)+f_{FD}\left(E_i(k)+\mu_i^*\right)\right] , \tag{12}$$

$$p_{kin} = \frac{1}{3}\sum_i \frac{2J_i+1}{2\pi^2}\int_0^\infty \frac{dk k^4}{E_i(k)} \cdot \left[f_{FD}\left(E_i(k)-\mu_i^*\right)+f_{FD}\left(E_i(k)+\mu_i^*\right)\right] . \tag{13}$$

Interaction terms exclusively depend on average values of mesonic fields

$$e_{meson} = \frac{m_\sigma^2}{2}\bar{\sigma}^2+\frac{m_\omega^2}{2}\bar{\omega}^2+\frac{m_\phi^2}{2}\bar{\phi}^2+\frac{m_\rho^2}{2}\bar{\rho}^2 , \tag{14}$$

$$p_{meson} = -\frac{m_\sigma^2}{2}\bar{\sigma}^2+\frac{m_\omega^2}{2}\bar{\omega}^2+\frac{m_\phi^2}{2}\bar{\phi}^2+\frac{m_\rho^2}{2}\bar{\rho}^2 . \tag{15}$$

The entropy density of baryonic matter writes

$$s_{baryon} = -\sum_i \frac{2J_i+1}{2\pi^2}\int_0^\infty dk k^2 \cdot \Big\{\Big[f_{FD}\left(E_i(k)-\mu_i^*\right)\ln f_{FD}\left(E_i(k)-\mu_i^*\right) + \bar{f}_{FD}\left(E_i(k)-\mu_i^*\right)\ln \bar{f}_{FD}\left(E_i(k)-\mu_i^*\right)\Big] + (\mu_i^* \to -\mu_i^*)\Big\} \tag{16}$$

Together with other thermodynamic quantities it verifies the thermodynamic identity

$$e_{baryon} = T s_{baryon} - p + \sum_i \mu_i n_i . \tag{17}$$

Matter composition is determined, at arbitrary thermodynamic conditions, by conservation of mass and charge,

$$n_B = \sum_i n_i, \tag{18}$$

$$n_Q = \sum_i q_i n_i, \tag{19}$$

along with chemical equilibrium. For the case of hyperon and Δ-admixed nucler matter chemical equilibrium conditions write,

$$\mu_n = \mu_\Lambda = \mu_{\Xi^0} = \mu_{\Sigma^0} = \mu_{\Delta^0} = \mu_B, \tag{20}$$

$$\mu_{\Sigma^-} = \mu_{\Xi^-} = \mu_{\Delta^-} = \mu_B - \mu_Q, \tag{21}$$

$$\mu_p = \mu_{\Sigma^+} = \mu_{\Delta^+} = \mu_B + \mu_Q, \tag{22}$$

$$\mu_{\Delta^{++}} = \mu_B + 2\mu_Q, \tag{23}$$

where μ_B and μ_Q stand for baryon and charge chemical potentials. Note that β-equilibrium is not assumed. Non-conservation of strangeness assumes $\mu_S = 0$.

Finally the interaction potential of particle j in k-particle matter is given by,

$$U_j^{(k)} = m_j^* - m_j + \mu_j - \mu_j^*, \tag{24}$$

$$= \Sigma_{S;j} + \Sigma_{V;j} + \Sigma_R. \tag{25}$$

As customarily in the literature throughout this paper couplings of heavy baryons to mesonic fields will be expressed as ratios to the corresponding couplings of nucleons. We shall also assume that the density dependencies of couplings of heavy baryons to mesonic fields are identical to the ones of nucleons.

4 Heavy Baryons at finite-T: the cases of Λ- and Δ-admixed nuclear matter

In the following we shall analyze the T- and n_B-dependence of various thermodynamic and microscopic quantities along with matter composition. The study will be performed for temperatures in the range $0.5 \le T \le 40$ MeV, neutron rich matter with $Y_Q = 0.3$ and two values of baryonic particle number density, $n_B = 0.4$ fm^{-3} and 0.6 fm^{-3}. The role of strange baryons and nucleonic resonances will be highlighted by confronting results of Λ- and Δ-admixed nuclear matter to results of purely nucleonic matter (N). For brevity in some circumstances only the characteristics of dominant species will be illustrated. The employed nucleonic interaction is DD2 [79].

The n_B and T-dependence of neutron, proton, Λ and Δs relative abundances is depicted in Fig. 1. Abundances of exotic species strongly depend on thermodynamic conditions and as a rule of thumb increase with T. At low (high) densities the abundances of Λ and Δ^-, which is the dominant member of the $J = 3/2$ quadruplet, show significant (negligible) dependence on T. Mass conservation and chemical equilibrium condition $\mu_n = \mu_\Lambda$ make that nucleation of Λ entails a certain diminish of neutron particle number densities, while no modification is seen in what regards X_p. The situation of Δ-admixed nuclear matter is more complex. The onset of Δ^- reduces X_n and enhances X_p. The first effect comes from mass conservation, while the latter is due to charge conservation and opposite charges of the dominant charged species, p and Δ^-. For the simple situations considered here one notices that abundances of exotic particles also increase with n_B.

The n_B and T-dependence of mesonic fields is addressed in Fig. 2. The following remarks are in order:

(a) N-matter: Being defined in terms of number densities of different particle degrees of freedom the average values of vector isoscalar ω and vector isovector ρ mesonic fields do not depend on temperature. The decrease of $\bar{\sigma}$ with T is due to the fact that, for any species i, the maximum contribution to the integrals in eq. (8a) is given by the k-values close to the solution of $\sqrt{k_i^2+m_i^{*2}} = \mu_i^*$ and that neutron and proton effective chemical potentials decrease with T, see Fig. 4.

(b) NΛ-matter: As already discussed, high T-values favor the production of Λs at the cost of neutrons, which ex-

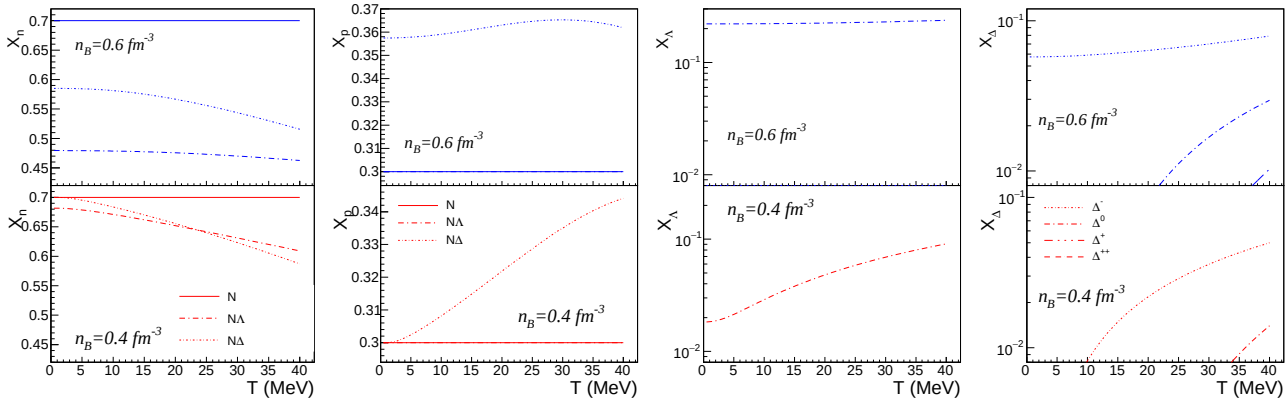

Fig. 1 T-dependence of relative particle abundances. Results corresponding to $N\Lambda$ and $N\Delta$-matter are confronted with those of nuclear matter (N) with $Y_Q = 0.3$ at $n_B = 0.4$ fm^{-3} and 0.6 fm^{-3}.

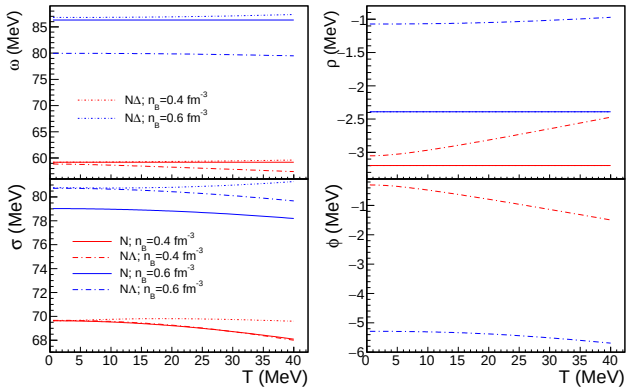

Fig. 2 T-dependence of mesonic fields. Results corresponding to N, $N\Lambda$ and $N\Delta$-matter with $Y_Q = 0.3$ at $n_B = 0.4$ fm^{-3} and 0.6 fm^{-3}.

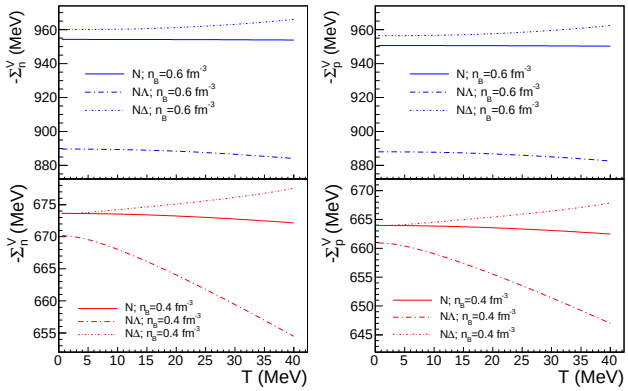

Fig. 3 Vector self energies of neutrons and protons, eq. (6), as function of T in nuclear matter (N) as well as $N\Lambda$ and $N\Delta$-matter with $Y_Q = 0.3$ at $n_B = 0.4$ fm^{-3} and 0.6 fm^{-3}.

plains that $|\bar{\phi}|$ augments with T and $|\bar{\rho}|$ diminishes with T. The latter feature suggests that, for fixed Y_Q, hot matter is more isospin symmetric than cold matter, in agreement with Fig. 1. Similarly to the case of $\bar{\sigma}(T)$ in N-matter and for the same reason $\bar{\sigma}$ and $\bar{\omega}$ decrease with T.

(c) $N\Delta$-matter: Similarly to Λs, also the production of Δs is favored by high temperatures and densities. Under the considered conditions, Δ^- is by far the most abundant species as its chemical potential, $\mu_{\Delta^-} = \mu_B - \mu_Q$, with $\mu_Q < 0$ is the largest. As $X_\Delta \ll X_\Lambda$, the average values of all mesonic fields in $N\Delta$ matter differ less with respect to their values in pure nucleonic matter than it was the case with $N\Lambda$. Qualitative differences of $\bar{\sigma}(T)$ and $\bar{\omega}(T)$ in $N\Delta$ with respect to $N\Lambda$ stem from opposite modifications of X_n and X_p, with the latter prevailing over the first.

$\bar{\sigma}$ and $\bar{\omega}$ augment with density as both scalar and vector number densities do so; the n_B-decrease of $g_{\rho B}$ explains the n_B-decrease of $|\bar{\rho}|$, the negative values being due to the fact that the matter is neutron rich. As the ϕ meson couples only to hyperons, $\bar{\phi} \neq 0$ only in $(N\Lambda)$ matter. Its absolute value increases with n_B as high densities favor production of strange particles.

The T-dependence of vector self-energies, eq. (6), at constant density is represented in Fig. 3; only the behavior of dominant species is illustrated. One notes that $-\Sigma^V_{n,p}$ strictly follow the T-evolution of dominant mesonic field ω, see Fig. 2. The strongest T-dependence is obtained for $N\Lambda$ matter at the lowest considered density, where chemical composition changes steeply.

The T-evolution of neutron and proton chemical potentials and effective chemical potentials is illustrated in Figs. 4 and, respectively, 5. With the exception of relatively abundant particles whose abundances augment with T, as is the case of protons in $N\Delta$-matter at $n_B = 0.4$ fm^{-3}, (effective) chemical potentials diminish with temperature. For neutrons, which represent the dominant species, a strong correlation exists between abundances and effective chemical potential. As in all cases considered here matter is neutron rich, $\mu_n > \mu_p$.

Eq. (3) states that the T- and n_B-dependence of the Dirac effective mass of any baryon is governed by the corresponding dependencies of $\bar{\sigma}$. $m^*_{n/p}(T, n_B)$ are illustrated in Fig. 6. Fig. 2 shows that Δ-admixed matter singles out by $\bar{\sigma}$ in-

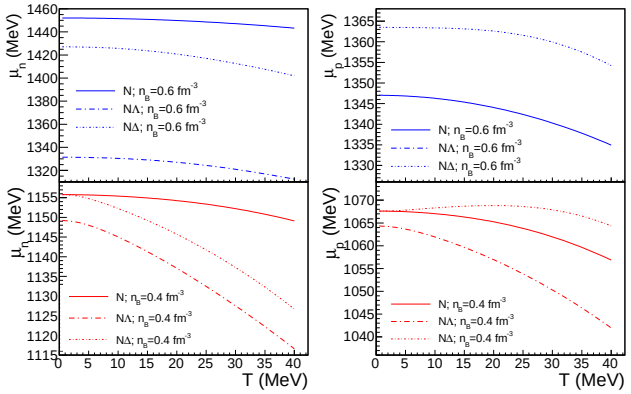

Fig. 4 Neutron and proton chemical potentials as function of T in nuclear matter (N) as well as $N\Lambda$ and $N\Delta$-matter with $Y_Q = 0.3$ at $n_B = 0.4$ fm^{-3} and 0.6 fm^{-3}.

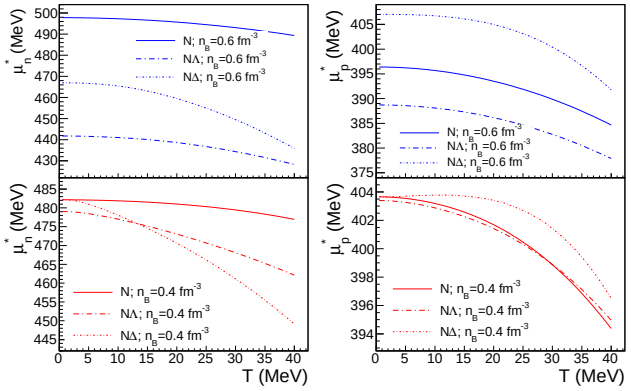

Fig. 5 The same as in Fig. 4 for neutron and proton effective chemical potentials, eq.(4).

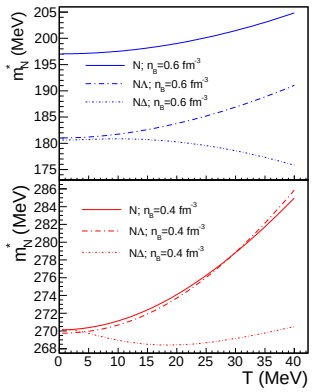

Fig. 6 T-dependence of nucleon Dirac effective mass, eq.(3), for the cases considered in Fig. 1.

creasing both with temperature and density. As such, contrary to what happens in nucleonic matter and Λ-admixed nuclear matter, in Δ-admixed nuclear matter the Dirac effective mass of nucleons decreases with density and, under specific thermodynamic conditions, also with temperature. The validity limit of the model is reached when nucleon effective Dirac masses vanish. For a parameter study of the maximum baryonic densities reachable in $N\Delta$-matter, see Sec. 5.

Contributions of different terms in eqs. (9) and (10) are illustrated in Figs. 7 and, respectively, 8 as function of T for different values of baryonic density and matter compositions.

In some cases, neutron and proton kinetic energy densities and pressures increase with T. These situations correspond to contributions of high momentum states in eqs. (12) and (13) that underscore the T-reduction of effective chemical potentials. For $N\Lambda$-matter at $n_B = 0.4$ fm^{-3} and $N\Delta$-matter the kinetic contribution of neutrons manifests an opposite behavior. These situations correspond to the cases where $\mu_n^*(T)$ shows a steep decrease, see Fig. 5. Quite remarkably, with the exception of protons in $N\Lambda$ matter at $n_B = 0.6$ fm^{-3}, the qualitative patterns of $e_{kin;n/p}(T)$ and $p_{kin;n/p}(T)$ as well as the relative arrangement of curves corresponding to different mixtures and/or baryonic densities is the same.

The T-dependence of p_{meson} shows a complex behavior: at high densities where mesonic fields show small variation with T, a tiny increase with T is obtained; for N- and $N\Delta$-matter with $n_B = 0.4$ fm^{-3}, p_{meson} increases with T; in the first (second) case this is mainly due to the decrease (increase) with T of $\bar{\sigma}$ ($\bar{\omega}$), see Fig. 2; for $N\Lambda$ matter with $n_B = 0.4$ fm^{-3}, p_{meson} has a non-monotonic behavior due to the interplay between $\bar{\sigma}$ and $\bar{\omega}$, both decreasing with T.

Similarly to p_{meson} at $n_B = 0.6$ fm^{-3} and for the same reasons also e_{meson} at $n_B = 0.6$ fm^{-3} shows a weak sensitivity to T. In what regards the behavior at $n_B = 0.4$ fm^{-3}, one notes that $e_{meson}(T)$ increases (decreases) in $N\Delta$ (N and $N\Lambda$) matter. Fig. 2 shows that this is the direct consequence of T-dependence of dominant $\bar{\sigma}$ and $\bar{\omega}$ fields.

For fixed densities, the T-dependence of the rearrangement pressure depends on the T-evolution of average mesonic fields. Little (strong) T-dependence of these fields at high (low) densities, see Fig. 2, explain the behavior shown in the right panel.

For the thermodynamic conditions under consideration here meson terms overshoot all other terms in e_{baryon} and p_{baryon}. Out of the different terms in eq. (10) the highest T-dependence is shown by p_{meson}. This means that, to a large extend, $p_{baryon}(T)$ will reflect the T-dependence of p_{meson}. The confirmation is provided by the right panel in Fig. 9. For $n_B = 0.4$ fm^{-3} $p_{baryon}^{(N\Lambda)}(T)$ has a U-shape, while in all other cases p_{baryon} increases with T. The left panels in Fig. 9 show that, in spite of the complex T-dependence of various terms entering eq. (9), e_{baryon} increases with T.

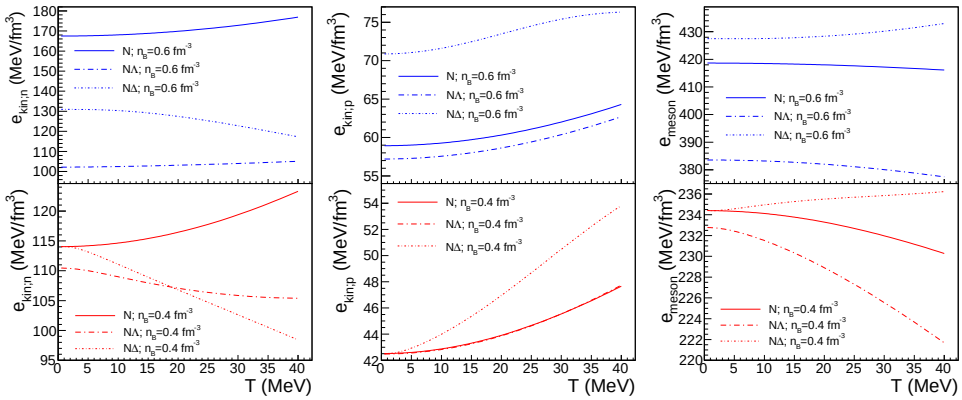

Fig. 7 T-dependence of different terms in eq. (9). Results corresponding to N-, $N\Lambda$- and $N\Delta$-matter with $Y_Q = 0.3$ at $n_B = 0.4$ fm^{-3} and 0.6 fm^{-3}.

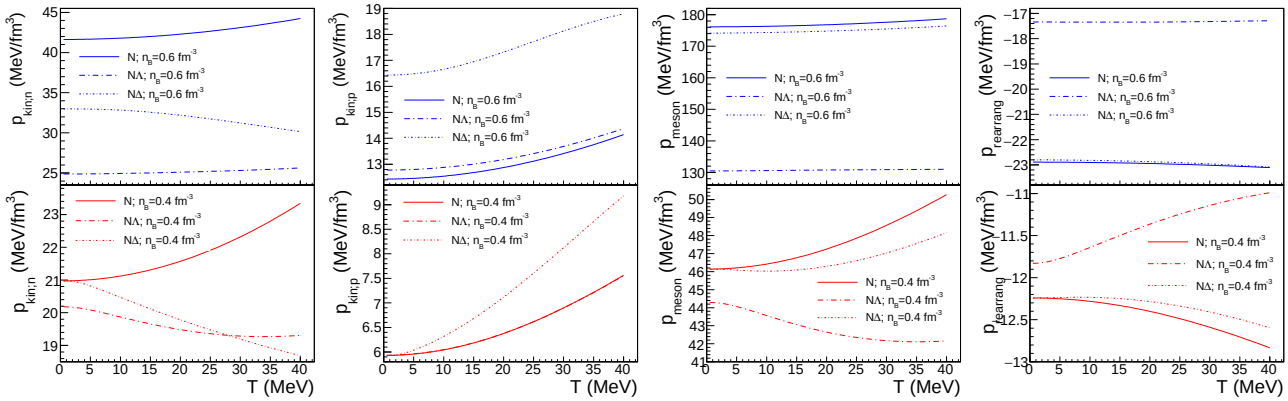

Fig. 8 The same as in Fig. 7 for different terms in eq. (10).

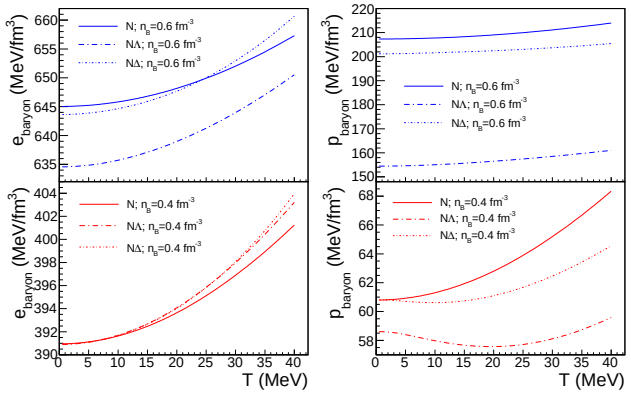

Fig. 9 T-dependence of energy density and pressure. Results corresponding to N-, $N\Lambda$- and ΔN-matter with $Y_Q = 0.3$ at $n_B = 0.4$ fm^{-3} and 0.6 fm^{-3}.

5 Thermodynamic stability of Δ-admixed nuclear matter: the case of $T = 0$

Within QCD the Delta-resonance is explained as a spin-isospin excitation of the nucleon into a $(J,I) = (3/2,3/2)$ configuration. Its strong coupling with the continuum of pion-nucleon p-wave scattering states explains its rapid decay in vacuum, within a half-life of about $t_{1/2} \approx 10^{-23}$ s. Due to the Pauli blocking, the Δs are nevertheless considered to be stabilized when embedded in a medium.

The fact that, contrary to other baryons, Δ-resonances are excited in various types of reactions [104], can in principle be exploited to constrain the interaction potential with nucleons. The data are nevertheless scarce such that the consequences of the onset of Δs in neutron stars are typically evaluated by allowing to the coupling constants of Δ to various mesonic fields to span wide ranges [105,106]. Herein the same modus operandi will be adopted.

Refs. [107,108] show that, if no other exotic degree of freedom is considered, nucleation of Δs reduces the maximum mass of NS by up to $\approx 0.5 M_\odot$ and radii of intermediate mass NS by up to ≈ 2 km. Both effects are due to the pressure decrease that accompanies the onset of any extra particle degree of freedom. The reduction of maximum mass reflects the reduction of pressure at baryonic densities equal to the values of the maximum mass configurations. The reduction of radii of intermediate mass NS reflects the evolution of pressure at the power $1/4$ at lower densities, typically $n_{sat} \lesssim n_B \lesssim 2n_{sat}$ [109]. If also hyperons are accounted for the only notable effect is the reduction of NS

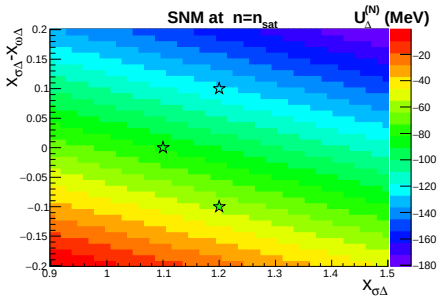

Fig. 10 Single-particle potential of Δ isobars in saturated symmetric nuclear matter, $U_\Delta^{(N)}(n_{sat})$, for $x_{\rho\Delta}=1$. The symbols correspond to the following sets of $(x_{\sigma\Delta},x_{\omega\Delta})$: (1.1,1.1), (1.2, 1.1), (1.2, 1.3) for which $U_\Delta^{(N)}=-83$ MeV, -124 MeV and -57 MeV.

radii [105,106,110,111,112,38]. The explanation resides in that, due to their attractive potential, Δs start nucleating at lower densities than the hyperons. The magnitude of these modifications nevertheless depends on the underlying nucleon effective interaction, strength of ΔN potential and Δs effective mass.

Most recently Ref. [44] has highlighted a series of other modifications. The first consists in the fact that, if the ΔN interaction potential is attractive enough, Δ-admixed nuclear matter becomes thermodynamically instable. These instabilities persist at finite temperatures and out of the β-equilibrium condition, which might in principle impact astrophysical scenarios like CCSN, collapse into a BH and BNS mergers [28, 29]. The second finding regards the shift of the nucleonic dUrca threshold to low densities, with obvious impact on the thermal evolution of isolated and accreting NS. This modification arises because Δ^-, which is the first Δ to be populated at β-equilibrium, partially supresses the neutralizing electron gas which, in turn, regulates the relative abundances of neutrons and protons. Though also these modifications depend on the strength of the Δ effective interaction they manifest over domains of the parameter space compatible with present astrophysical constraints.

In this section we shall investigate the following aspects: i) the dependence of the Δ-potential in nuclear matter and ii) the maximum value of baryonic particle number density on Δ couplings to mesonic fields, iii) thermodynamic instabilities of cold $N\Delta$ and $N\Delta e$ matter. For ii) and iii) the limiting values $Y_Q=0.01$ and 0.5 will be considered. As in Ref. [44] hyperons and muons are disregarded for simplicity. As [105,106,110,111,112] we shall allow the strength functions to cover wide domains of values, $0.90\leq x_{\sigma\Delta}\leq 1.50$, $-0.20\leq x_{\sigma\Delta}-x_{\omega\Delta}\leq 0.20$. For brevity $x_{\rho\Delta}=1$. For nucleons the DD2 [79] effective interaction is employed; note that this interaction is different than the one used in [44].

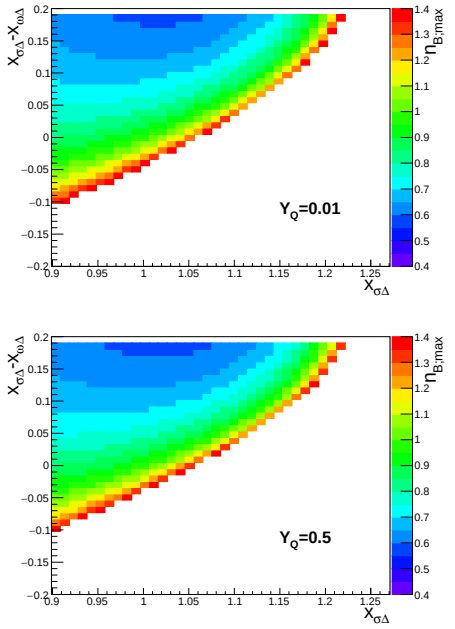

Fig. 11 Maximum reachable value of n_B (in fm^{-3}) in cold Δ-admixed nuclear matter with $Y_Q=0.01$ (top) and $Y_Q=0.5$ (bottom), determined by vanishing nucleon Dirac effective mass.

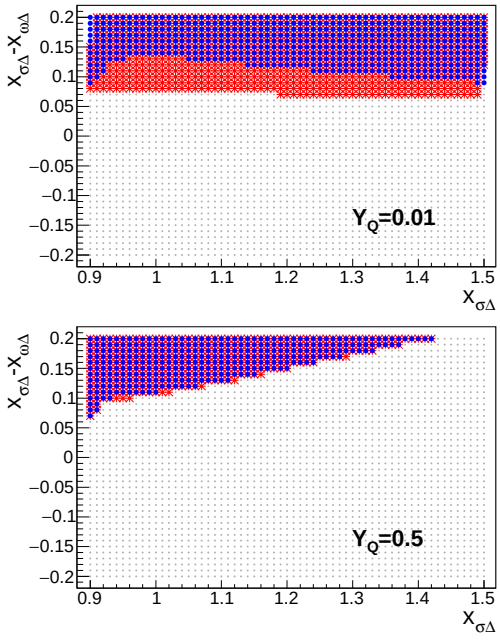

Fig. 12 Parameter sets which allow for Δ-driven spinodal instabilities in cold (N,Δ) (red) and (N,Δ,e) (blue) matter with $Y_Q=0.01$ (top) and $Y_Q=0.5$ (bottom).

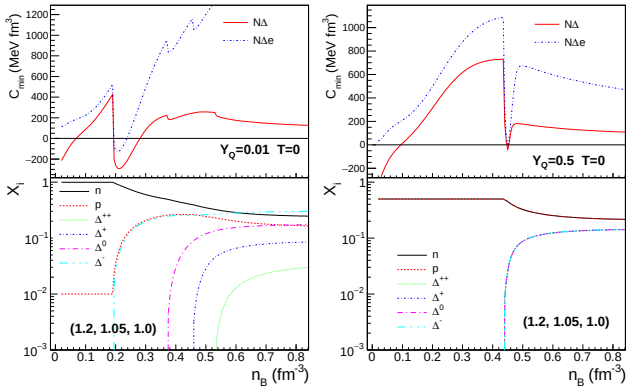

Fig. 13 Top: Minimum value of the curvature matrix as function of n_B in cold Δ-admixed nuclear matter; results corresponding to pure baryonic matter (baryonic matter plus electrons) are illustrated with red (blue) lines. Bottom: Relative particle abundances as function of n_B. Left (right) panels correspond to $Y_Q = 0.01$ ($Y_Q = 0.5$). The values of coupling constants are mentioned on the figure.

5.1 $U_\Delta^{(N)}$ potentials

The well depth of the Δ-potential in nuclear matter writes [2]

$$U_\Delta^{(N)} = -g_{\sigma\Delta}\bar{\sigma} + g_{\omega\Delta}\bar{\omega} + g_{\rho\Delta}t_3\bar{\rho} + \Sigma_R, \quad (26)$$

where t_3 is the third component of the isospin, with the convention $t_{3\Delta^{++}} = 3/2$. [Herein the baryonic particle number density dependence of the potential, coupling constants, rearrangement term and mesonic fields has been omitted.] Eq. (26) shows that large values of $g_{\sigma\Delta}$ and low values of $g_{\omega\Delta}$ entail more attractive potentials. It also shows that in neutron rich matter, where $\bar{\rho} < 0$, the potential felt by positively charged isobars is larger in absolute values than the one felt by negative isobars. In symmetric nuclear matter, where $\bar{\rho} = 0$, all isobars experience the same potential.

Experimental data from pion-nucleus scattering and pion photo-production, electron scattering on nuclei and electromagnetic excitation of the Δ-baryons, compiled by [105, 106], have been translated into a Δ-potential at rest in nuclear matter slightly more attractive than the one of nucleons, $-30\,\mathrm{MeV} + U_N^{(N)} \lesssim U_\Delta^{(N)} \lesssim U_N^{(N)}$. Recent analysis of inclusive quasi-elastic electron scattering data on nuclear targets [113] led to $U_\Delta^{(N)} \approx 1.5 U_N^{(N)}$, which corresponds to the maximum attraction boundary cited above. Comparison between experimental pion production data in energetic heavy ion collisions and results of a quantum molecular transport model have been exploited in order to extract, in addition to the isoscalar Δ potential, also the isovector component [114]. The results reveal correlations of these two components with the value of Landau effective mass of Δ and slope of the symmetry energy.

Fig. 10 illustrates the range of values spanned by $U_\Delta^{(N)}$ in saturated symmetric nuclear matter. It comes out that $U_\Delta^{(N)}(n_{\rm sat})$ is degenerate with respect to these two coupling constants and for all considered combinations $(x_{\sigma\Delta}, x_{\omega\Delta})$ the potential is attractive. The values taken by $U_\Delta^{(N)}(n_{\rm sat})$ when the coupling constants take the values employed by the three new general purpose EoS models proposed in this paper, see Sec. 2, are signaled by symbols. For $(1.1, 1.1, 1.0)$ $U_\Delta^{(N)}$ falls in the domain $-30\,\mathrm{MeV} + U_N^{(N)} \lesssim U_\Delta^{(N)} \lesssim U_N^{(N)}$ [105, 106], while more (less) attraction is obtained for $(1.2, 1.1, 1.0)$ [$(1.2, 1.3, 1.0)$].

5.2 Maximum baryonic particle number density

Refs. [115, 116] showed that, for wide domains of the parameter set, the maximum mass of Δ-admixed NS is much lower than the one corresponding to nucleonic NS built upon the same effective nucleonic interaction. [44] showed that this does not stem from the softening of the $P(e)$ EoS upon nucleation of Δ^- but from the inability to reach baryon densities high enough to sustain massive NS, due vanishing nucleon Dirac effective masses. For the Δ-induced modifications of m_N^*, see Sec. 4. EoS models falling in this situation will obviously not meet the lower bound on NS maximum mass [47] and should be ruled out.

Maximum values of n_B allowed by different combinations of $(x_{\sigma\Delta}, x_{\omega\Delta})$ but smaller than (the arbitrarily chosen value) 1.4 fm^{-3} are depicted in Fig. 11. The panels corresponding to $Y_Q = 0.5$ and 0.01 are very similar, as expected due to the weak sensitivity of the $\bar{\sigma}$ to the isospin asymmetry. The color levels show that high enough values of $n_{B;max}$ may be reached for any value of $x_{\sigma\Delta}$ provided that $x_{\omega\Delta}$ is tuned accordingly. Some of the thus selected sets of parameters will though not agree with constraints on $U_\Delta^{(N)}$, see Sec. 5.1.

5.3 Thermodynamic (in)stabilities

Sufficiently attractive interaction potentials are known to lead to thermodynamic instabilities. The best documented example in nuclear physics corresponds to sub-saturated nuclear matter where a liquid-gas like phase transition is predicted by a large variety of models, including phenomenological non-relativistic [117, 118, 119] and relativistic [120, 121] mean field models and microscopic approaches [122, 123]. This phase transition is nevertheless not expected to play a role in NS or core-collapse supernovae as it is suppressed by the neutralizing electron gas. According to [124, 125, 126,

[2] Eq. (26) corrects eq. (1) in [44], where the rearrangement term has been omitted. The calculations in [44] have been nevertheless performed with the correct expression.

127] strangeness-driven instabilities may manifest in suprasaturated matter and, contrary to the case discussed above, are not significantly altered by electrons such that they might be explored along the β-equilibrium path as well as out of β-equilibrium in the neutrino transparent matter. In lack of sufficient knowledge of effective baryon interactions in strangeness $S=1$ and 2 channels this possibility nevertheless remains speculative. Ref. [116,44] proved that CDFT models allow for Δ-driven instabilities in NS matter. These instabilities might occur for strength parameters in accord with available data and extend over a narrow density domain at densities slightly exceeding n_{sat}.

Spinodal instabilities manifest as convexity anomalies of the thermodynamic potential and are mathematically signaled by negative values of the curvature matrix $C_{i,j}=\partial\mu_i/\partial n_j$, where μ and n stand for the chemical potential and number density of the two conserved charges $i,j=B,Q$.

We extend here the investigation performed in [44] to matter with fixed charged fraction. Properties of purely baryonic matter and mixture of baryons and electrons with $Y_Q=Y_e$ are confronted in Fig. 12. The cases $Y_Q=0.01$ and 0.5 are considered. Δ-driven instabilities exist for both systems; the parameter sets which allow for them are more numerous for $Y_Q=0.01$ than for $Y_Q=0.5$. This first result is counterintuitive as the domain of thermodynamic instabilities in dilute nuclear matter shrinks as Y_Q diminishes. It can nevertheless be understood considering that production of Δs, in particular Δ^-, is favored by small Y_Q-values. Indeed, Fig. 13 shows that the Δ onset occurs at $n_B\approx 0.2$ fm^{-3} ($n_B\approx 0.42$ fm^{-3}) for $Y_Q=0.01$ ($Y_Q=0.5$). Moreover at large densities, Δs are relatively more important in matter with low Y_Q-values. Fig. 12 also shows that the neutralizing electron gas has almost no consequence at $Y_Q=0.5$ while at $Y_Q=0.01$ it suppresses the instabilities for $0.05\lesssim x_{\sigma\Delta}-x_{\omega\Delta}\lesssim 0.1$. Having in mind the behavior of dilute nuclear matter also this result is surprising. It can nevertheless be explained considering that the surface of the thermodynamic potential is altered more by the early and strong production of Δs in matter with low Y_Q, see bottom panels of Fig. 13. Finally the density domains affected by instabilities are wider in matter with low Y_Q.

We note that, when the contribution of the electron gas is accounted for, none of the models of $Y\Delta$-admixed matter introduced in this paper manifests instabilities. At variance with this pure baryonic matter is stable [unstable] for $(1.1,1.1,1.0)$ and $(1.2,1.1,1.0)$ [$(1.2,1.3,1.0)$].

6 Finite temperature behavior

In this section we shall analyze thermal properties of a bunch of selected models accounting for various particle d.o.f. The behavior of baryonic matter and/or stellar matter, which means with lepton and photon gases contributions included, will be considered. Properties of pure baryonic matter are inferred from the corresponding tables on CompOSE database or, when these are not available, by subtracting from the values corresponding to stellar matter the contribution of lepton and photon gases.

For each quantity we shall start by commenting the behavior of purely nucleonic matter seen in Paper I.

6.1 Energy density and pressure

Thermal effects on thermodynamic state variables like energy density and pressure are conveniently highlighted by considering the difference between the finite temperature and the zero temperature quantity

$$X_{th}=X(n_B,Y_e,T)-X(n_B,Y_e,0)\ . \tag{27}$$

In Paper I we have shown that in the limit of vanishing density the baryonic thermal energy density e_{th} and pressure p_{th} approach zero and have no EoS-dependence, which means that whenever the interactions are weak the system recovers the ideal gas behavior; beyond this limit a strong EoS-dependence exists; at $n_B\gtrsim 1$ fm^{-3} the dispersion between non-relativistic (relativistic) models is large (small); the relative significance of thermal effects is more important at low densities than at high densities; pressure is more sensitive to T than energy; non-relativistic and relativistic models manifest different patters of the n_B-dependence of thermal energy density and pressure. The latter feature is attributable to the different expressions of single particle energies in the two classes of models together with the different density dependencies of the effective masses they depend on. In agreement with previous findings in [128,129] Paper I showed that in non-relativistic models e_{th} depends on the Landau effective mass while p_{th} depends on both Landau effective mass and its density dependence. In relativistic models the correlation between e_{th} and p_{th} and Dirac effective mass appears in that models with similar (different) density dependencies of this quantity produce similar (different) thermal effects. This feature is visible also in Figs. 14 and 15, where thermal effects in HS(DD2) are similar to those in STOS(TM1) and different from those in SFHo.

Figs. 14 and 15 further analyze the role of exotic particle d.o.f., hyperons, Δ-resonances, π, K^- and quarks, on baryonic thermal energy density $e_{th}(n_B)$ and pressure $p_{th}(n_B)$ at various thermodynamic conditions. Predictions of models allowing for exotica are confronted with those of purely nucleonic counterparts.

Fig. 14 shows that, similarly to what happens for purely nucleonic matter, also in matter which accounts for extra particle d.o.f. e_{th} augments with n_B and T. Nucleation of exotic particles makes e_{th} increase with respect to its value in nucleonic matter and the larger the number of particle d.o.f.

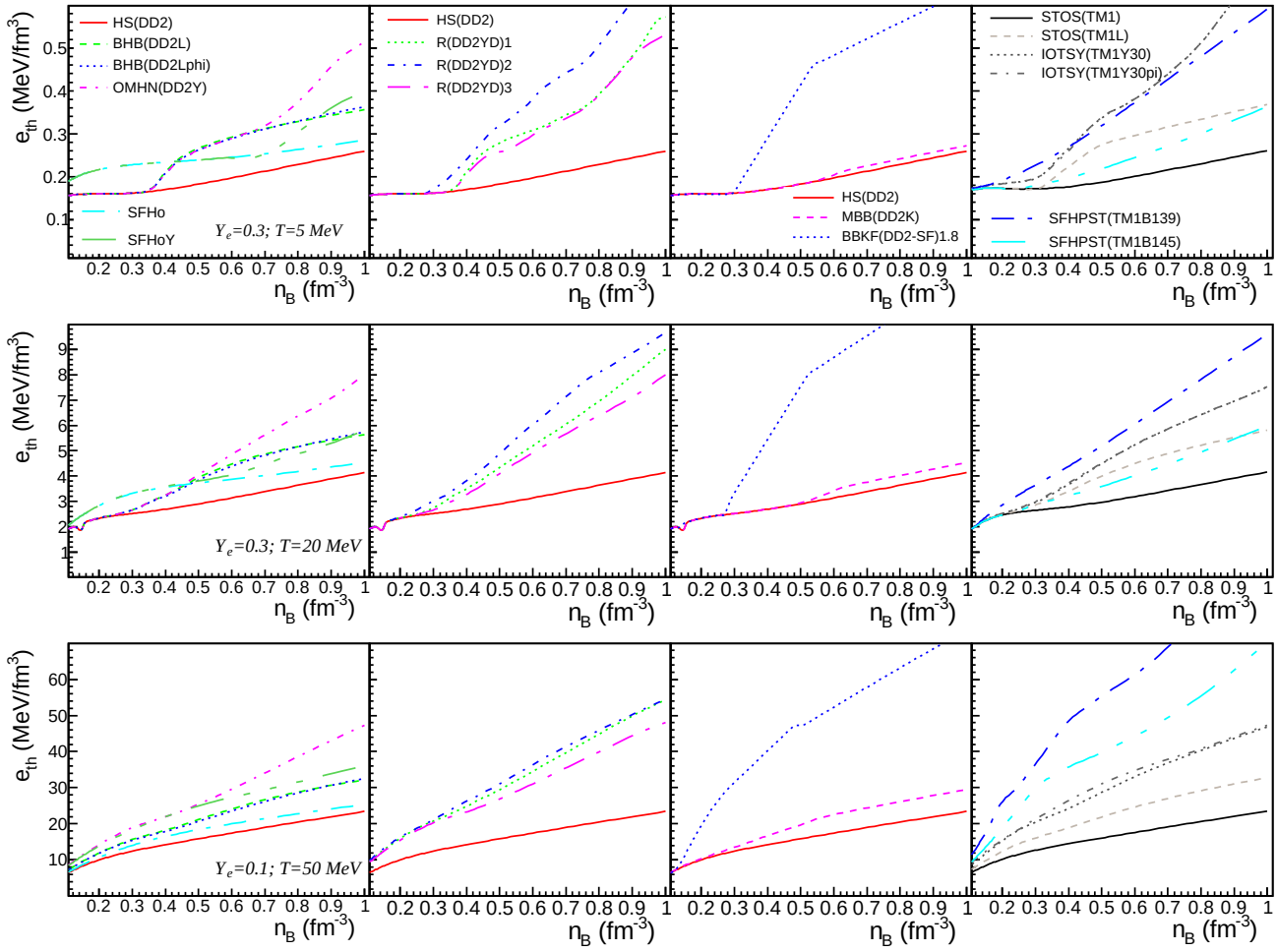

Fig. 14 Baryon (quark) contribution to the thermal energy density e_{th}, eq. (27), as function of baryon number density for ($Y_e = 0.3$, T=5 MeV) (top), ($Y_e = 0.3$, T=20 MeV) (middle) and ($Y_e = 0.1$, T=50 MeV) (bottom). The results are depicted for various EoS models. The indices 1, 2 and 3 of R(DD2YDelta) models refer to the following sets of couplings of Δ to σ, ω and ρ mesonic fields: (1.1, 1.1, 1.0), (1.2, 1.1, 1.0), (1.2, 1.3, 1.0).

the more significant this increase is. Indeed, for whatever T and n_B, e_{th} is larger for R(DD2YDelta) than for OMHN(DD2Y), which in turn is larger than for BHB(DD2L), which in turn is larger than for HS(DD2); predictions of e_{th} by MBB(DD2K) and HS(DD2); IOTSY(TM1Y30pi), IOTSY(TM1Y30), STOS(TM1L) and STOS(TM1); SFHPST(TM1b139) and STOS(TM1) obviously comply to the same rule. The steep (smooth) increase of exotic particle abundances at low (high) temperature results in an abrupt (smooth) variation of $e_{th}(n_B)$. Confrontation of predictions of MBB(DD2K) [69] with those of HS(DD2) [64] shows that significant effects related to K^- are obtained only at temperatures of the order of several tens MeV. Confrontation of predictions of IOTSY(TM1Y30pi) and IOTSY(TM1Y30) [61] shows that even at high temperatures the pions play little role. Within BBKF(DD2-SF)1.8 [77] e_{th} in quark matter is very high and, in the mixed phase, increases linearly with n_B; the fact that the temperature affects more the quark matter than its hadron counterpart is due to the low mass of quarks. In BBKF(DD2-SF) models [77] pure hadron and quark phases in coexistence have equal values of T, P, μ_B and Y_Q (instead of μ_Q). The latter feature explains that along trajectories of constant-Y_Q quantities calculated in the coexistence phase as linear combinations of values at the borders, as it is the case of e_{th}, manifest linear behaviors. In what regards the width and localization of the phase coexistence domain, no significant T-dependence is observed. Relying on a Glendenning construction [97] SFHPST models [62] manifest other features than those previously seen for BBKF(DD2-SF) models [77]. In the mixed phase e_{th} is not a linear function of n_B; straightforward identification of density domains populated by different phases is not possible; the curves corresponding to SFHPST models resemble qualitatively the curves of models with heavy baryons, which feature no phase transition. Results of BBKF(DD2-SF)1.8 and SFHPST are similar only in the very high values of e_{th} obtained at $T = 50$ MeV. We also note that the model with small value of the bag con-

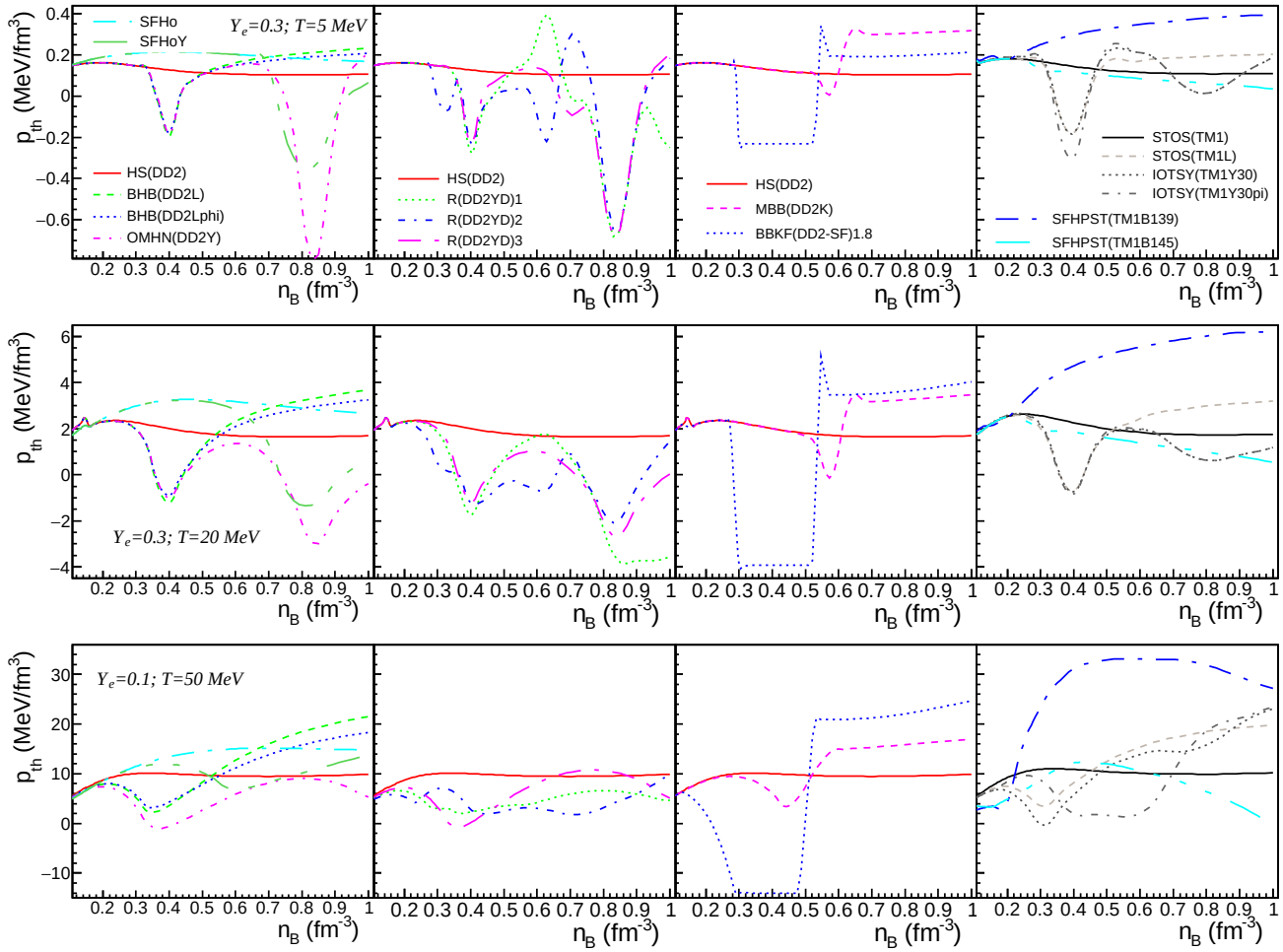

Fig. 15 Same as fig. 14 for the baryon (quark) contribution to the thermal pressure.

stant, which allows for an early transition to quark matter, manifests also larger thermal contributions.

We have seen in Fig. 9 that under specific thermodynamic conditions $p^{(N\Lambda)}_{baryon}$ and $p^{(N\Delta)}_{baryon}$ decrease with T, which translates into negative values for the baryonic component of p_{th}. Figs. 15 confirms that nucleation of exotic species results in a strong reduction of the baryonic component of p_{th} and that under specific conditions this quantity becomes negative. Competition with increasing values of baryonic chemical potential, which favor higher p_{th}-values, explains the strongly fluctuating behavior of this quantity over the considered density domain for all EoS models which account for heavy baryons and K^-. The quark phase in BBKF(DD2-SF)1.8 [77] is characterized also by large values of p_{th}, in addition to the large values of e_{th} discussed earlier and, with the exception of a narrow domain neighboring the hadron-quark coexistence, p_{th} increases with n_B. Equality of temperature, pressure and Y_Q between pure hadron and quark phases, assumed by the (approximate) Gibbs construction, explains that in the coexistence domain $p_{th;baryon}(n_B)$ curves at constant-T feature a plateau. The narrow peak at the border between phase coexistence and quark phase is likely a numerical artifact. No plateau is present in the mixed phase domain of SFHPST-models. This is due to the fact that mechanical equilibrium is imposed not among pure phases at the boundaries of the phase coexistence region but between different phases in the coexistence domain. The evolution with n_B is smooth but not necessarily monotonic. As for e_{th}, models with small bag constants lead to large thermal effects on p_{th}. Overall p_{th} manifests strong dependence on EoS, temperature and baryonic density. The only situation in which a particle is seen to play a little role corresponds to pions at temperatures of the order of a few tens MeV or lower.

6.2 Thermal index

The strong EoS- and density dependence of e_{th} and p_{th} seen in Paper I spurred us to further investigate the reliability of the so-called Γ_{th}-law, customarily employed in numerical

simulations [130,131,9,132,24] in order to supplement cold EoS with finite temperature contributions. The behavior of the Γ-factor defined as

$$\Gamma_{th} = 1 + \frac{p_{th}}{e_{th}} \,, \tag{28}$$

was analyzed separately for baryonic and stellar matter. In each case values of realistic EoS models have been compared with limiting values of idealized systems as well as with the domain of values, $1.5 \leq \Gamma_{th} \leq 2$, employed in simulations. The conclusions of Paper I dealing with nucleonic models can be summarized as follows: i) at high temperatures and low densities, where the ideal gas behavior is recovered, $\Gamma_{th;baryon} \to 5/3$, where $5/3$ is the classical limit for a dilute gas, ii) relativistic models provide for high n_B-values, $\Gamma_{th;baryon} \approx 4/3$, where $4/3$ corresponds to ultra-relativistic gases, iii) at high densities predictions of relativistic and non-relativistic models differ qualitatively and quantitatively, iv) over wide but EoS-dependent domains of (n_B, T), $\Gamma_{th;tot} > 2$ or $\Gamma_{th;tot} < 1.5$.

The behavior of the Γ_{th} factor for stellar matter is investigated in Fig. 16. Predictions corresponding to different EoS models and various thermodynamic conditions are considered. As in Paper I, we obtain a strong EoS-, T- and n_B-dependence of $\Gamma_{th;tot}$. The minima in $p_{th}(n_B)$, see Fig. 15, lead to one or several minima in $\Gamma_{th;tot}(n_B)$; the negative values of p_{th} lead, for the lowest considered temperature, to negative values of $\Gamma_{th;tot}$. The hadron-quark coexistence region of BBKF(DD2-SF)1.8 singles out by Γ_{th}-values significantly smaller than those obtained in pure hadron and quark phases. The SFHPST-models show rather smooth but non-monotonic $\Gamma_{th;tot}(n_B)$ curves.

The upper value $\Gamma_{th} = 2$ used in simulations is exceeded only over narrow density domains and only by some of the models allowing for Δ, K^- and quarks; at variance with this all models predict $\Gamma_{th} < 1.5$ over broad ranges of densities, where 1.5 is the lower limit assumed in simulations. The departure from $1.5 \leq \Gamma_{th}$ is more significant for exotic matter than it was for nucleonic matter.

6.3 Chemical potentials

The impact of composition changes on baryon and charge chemical potentials is addressed in Figs. 17 and 18. Fig. 17 confirms what we have seen in Fig. 4 (left panel) for the simpler cases of $N\Lambda$ and $N\Delta$ matter. Namely that exotic particles are created at the cost of neutrons, which make $\mu_B = \mu_n$ decrease. At low temperatures, predictions of OMHN(DD2Y) are identical to those of BHB(DD2Lphi) and differ from those of BHB(DD2L); this suggests that the repulsion mediated by the exchange of ϕ mesons dominates over modifications induced by Σs and Ξs. Predictions of other hyperonic models based on the same nucleonic EoS model are very similar (slightly different) at low (high) T. At both low and high temperatures the three models corresponding to $NY\Delta$-matter provide almost the same $\mu_B(n_B)$ in spite of notable differences in chemical composition. The equality of baryon chemical potentials and Y_Q-values in the hadron and quark phases imposed by the approximate Gibbs construction in BBKF(D2-SF)1.8 explains the plateau in the curves belonging to this model; by increasing T this plateau gets wider and shifts to lower densities; the information thus extracted from $\mu_B(n_B)$ at constant T corrects the one previously extracted from the less thermodynamically relevant e_{th} and p_{th} as function of n_B at constant T, see Figs. 14 and 15. No particular structure suggestive for phase coexistence manifests in the curves of SFHPST-models.

The partial replacement of neutrons by exotic particles also makes $|\mu_Q|$ decrease, see Fig. 18. The most dramatic modifications are obtained for models with large-L values. As with $\mu_B(n_B)$, at $T = 5$ MeV the predictions of OMHN(DD2Y) coincide with those of BHB(DD2Lphi) and differ from those of BHB(DD2L). At $T = 50$ MeV and $Y_Q = 0.1$ the largest departure from the predictions of nucleonic models is obtained for the following models: OMHN(DD2Y), the three R(DD2YD)-models; IOTSY(TM1Y), IOTSY(TM1Ypi); MBB(DD2K); the two SFHPST-models. For the first listed models the explanation relies in the presence of negatively charged exotic species. For SFHPST(TM1) the explanation relies in the negatively charged strange quark. The fact that in BBKF(D2-SF)1.8 the phase construction is performed at constant Y_Q explains why μ_Q is not constant in the hadron-quark coexistence region. The similar charge fractions of the coexisting phases [77] nevertheless makes that the slope of $\mu_Q(n_B)$ is small. As for $\mu_B(n_B)$, $\mu_Q(n_B)$ of SFHPS-models feature no plateau.

We also note that in warm Y-, $Y\Delta$- and K^--admixed matter with densities exceeding a certain value $\mu_Q > 0$, which means that $n_n < n_p$. Over two density domains also SFHPST(TM1B139) predicts that for $T = 50$ MeV and $Y_Q = 0.1$ $\mu_Q \gtrsim 0$; whenever this is the case the number of up quarks exceeds the one of down quarks.

Before leaving this section let us note that, for nucleonic models, EoS stiffness and density dependence of the symmetry energy impact the high density values of baryon and charge chemical potentials. Indeed, the highest (smallest) value of μ_B corresponds to DD2 (TM1), which provides the stiffest (softest) model. Similarly, for isospin asymmetric nuclear matter DD2 (TM1), with a low (high) L-value, provides small (large) values of $|\mu_Q|$.

6.4 Entropy, specific heats, adiabatic index, speed of sound

Further insight into the impact of exotic particle d.o.f. on thermodynamic quantities is offered in Fig. 19. It shows the baryonic entropy per baryon for (T=5 MeV, $Y_e = 0.3$)

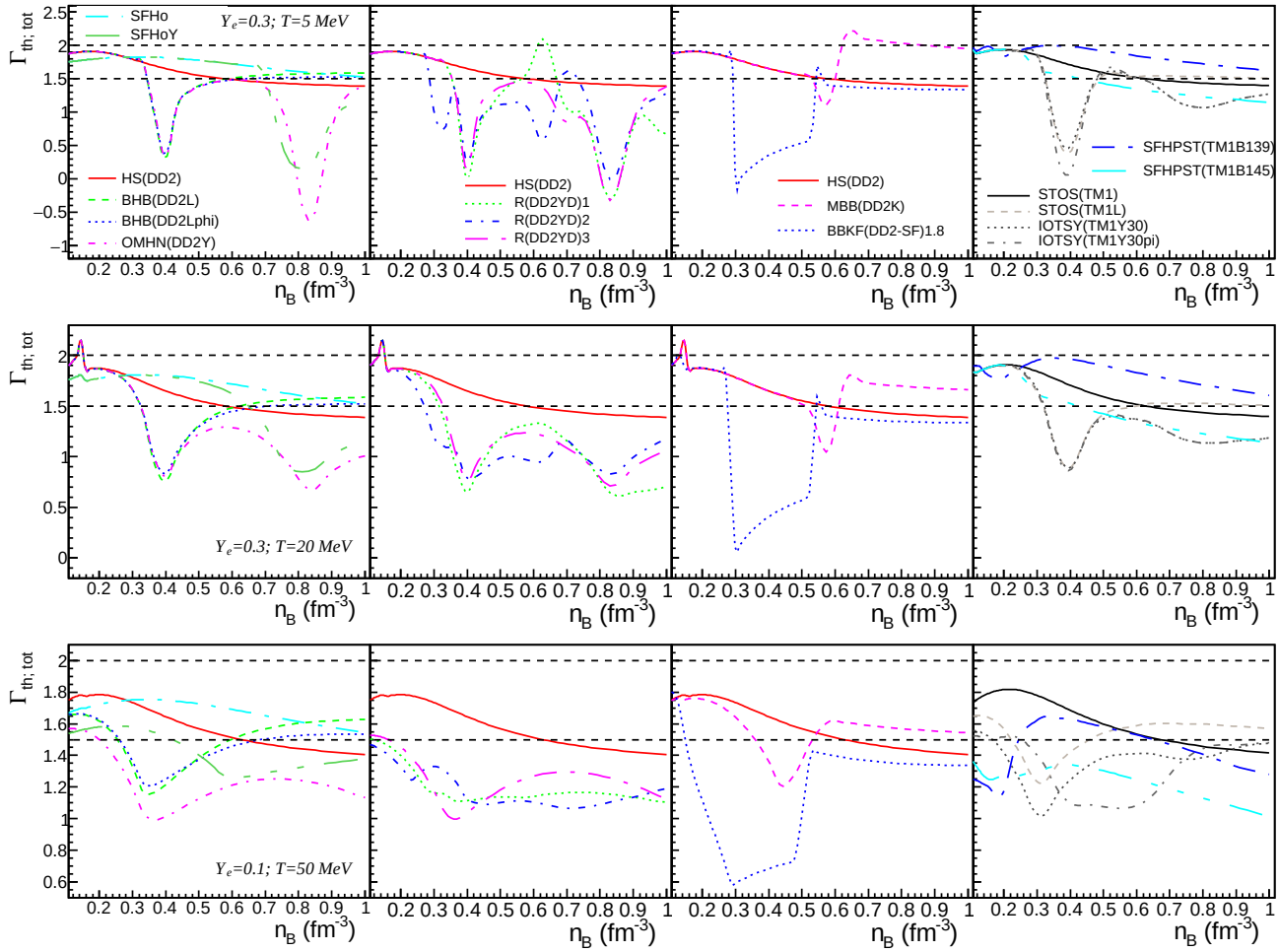

Fig. 16 Γ_{th}, eq.(28), as function of baryon number density at (T=5 MeV, $Y_e = 0.3$), (T=20 MeV, $Y_e = 0.3$), (T=50 MeV, $Y_e = 0.1$). Results corresponding to stellar matter (contributions of lepton and photon gases are included). Dashed horizontal lines mark the values $\Gamma_{th} = 1.5$ and 2.

and (T=50 MeV, $Y_e = 0.1$). As already seen and commented at length in Paper I, at fixed T in models with nucleonic d.o.f. S/A decreases with n_B. The same holds true for models with heavy baryons and/or K^-, π at high temperatures. At fixed T and n_B, S/A increases with the number of particle species. The steep increase in the abundance of newly populated species, as it happens with heavy baryons and K^- at low T, results in bumps of $S/A(n_B)$. As it was the case with $e_{th}(n_B)$ pions do not alter $S/A(n_B)$ when added to hyperons within IOTSY with $U_\Sigma^{(N)} = 30$ MeV. The non-monotonic $S/A(n_B)$ in BBKF(DD2-SF)1.8 results from the first order transition between the hadron and quark phases, the latter being characterized by much larger values of S/A. Curves belonging to SFHPST-models are qualitatively similar to those produced by models with heavy baryons. The dispersion between the different curves increases with T as so does the dispersion between chemical compositions. At high-T models accounting for quarks deviate the most from the predictions of the nucleonic counterparts.

The specific heat at constant volume is defined as

$$C_V = T\frac{\partial\,(S/A)}{\partial T}|_{V,\{N_i\}}\ . \tag{29}$$

Fig. 20 illustrates the evolution of C_V as function of baryon number density for different thermodynamic conditions. As easy to anticipate based of the definition, eq. (29), $C_V(n_B)$ replicates the behavior of $S/A(n_B)$. Under specific thermodynamic conditions models which employ for the sub-saturation density domain the extended NSE calculations in [64] show discontinuities over $n_{sat}/2 \lesssim n_B \lesssim n_{sat}$. These are numerical artifacts of the way in which the transition from clusterized to homogeneous matter was dealt with and have no physical ground.

The behavior of the adiabatic index, defined as

$$\Gamma_S = \frac{\partial \ln P}{\partial \ln n_B}|_S = \frac{C_P}{C_V}\frac{n_B}{P}\frac{\partial P}{\partial n_B}|_T\ , \tag{30}$$

is illustrated in Fig. 21 for stellar matter, *i.e.* with the contributions of leptons and photons included. The predictions by

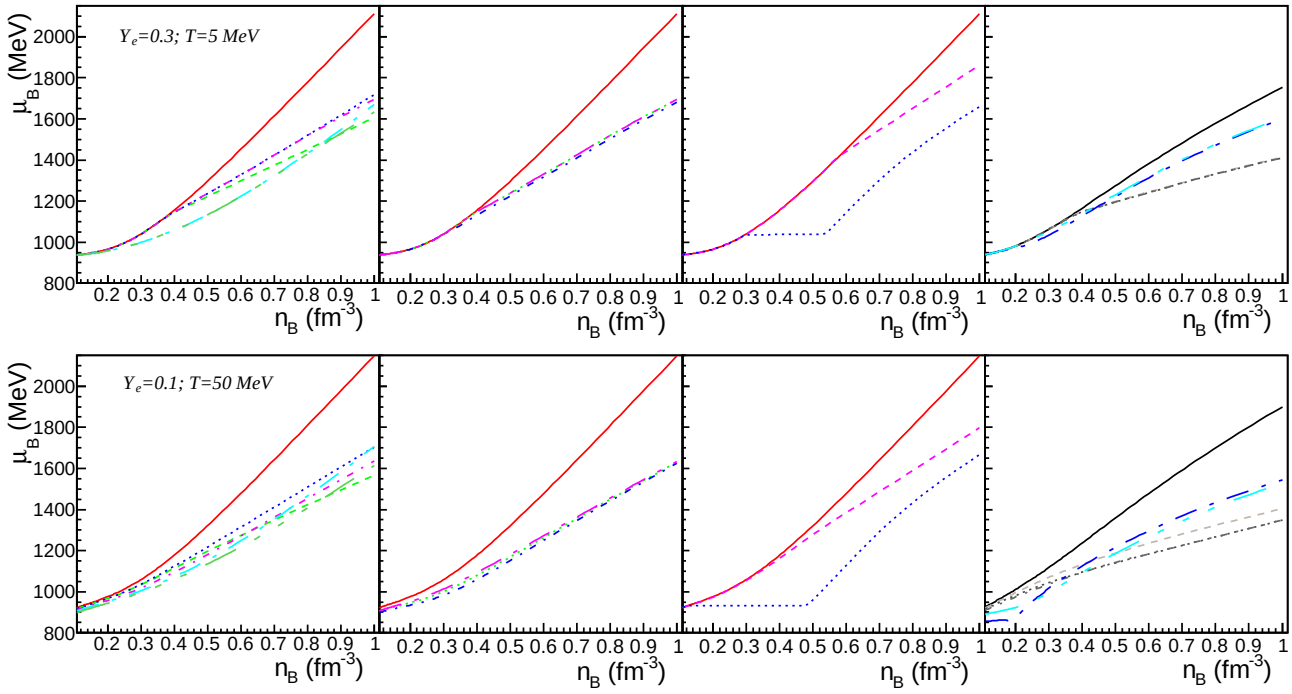

Fig. 17 Baryon chemical potential as function of baryon number density at (T=5 MeV, $Y_e = 0.3$) and (T=50 MeV, $Y_e = 0.1$). The key legend is as in Fig. 14.

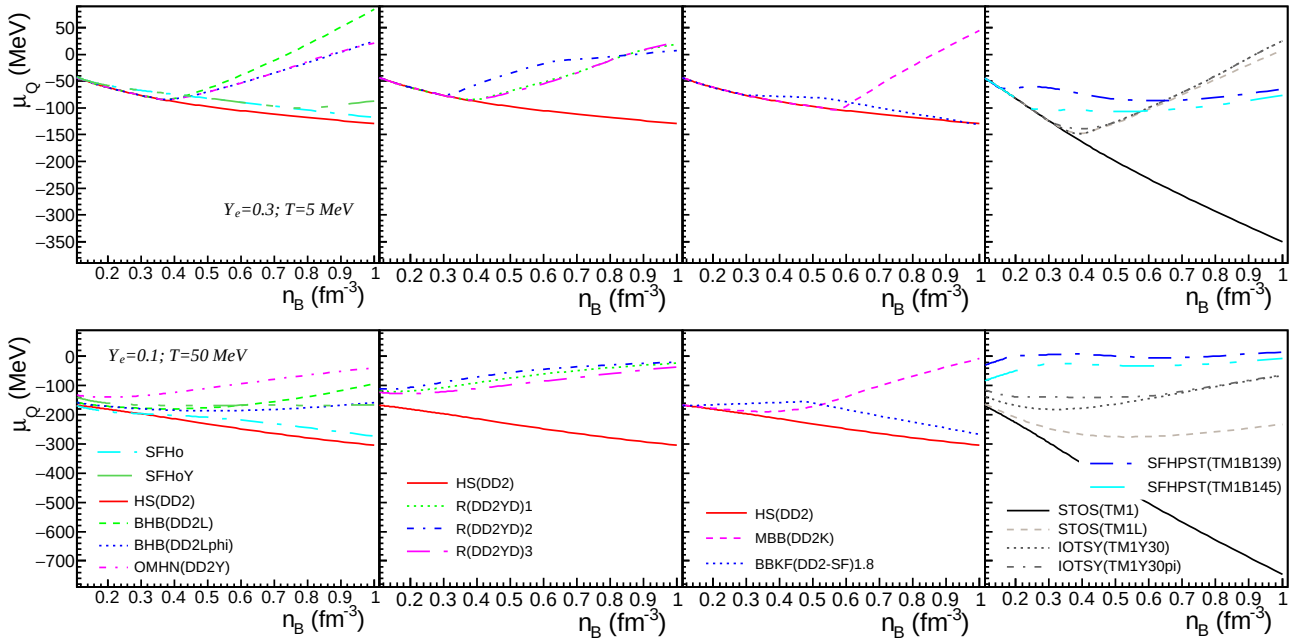

Fig. 18 The same as in Fig. 17 for charge chemical potential.

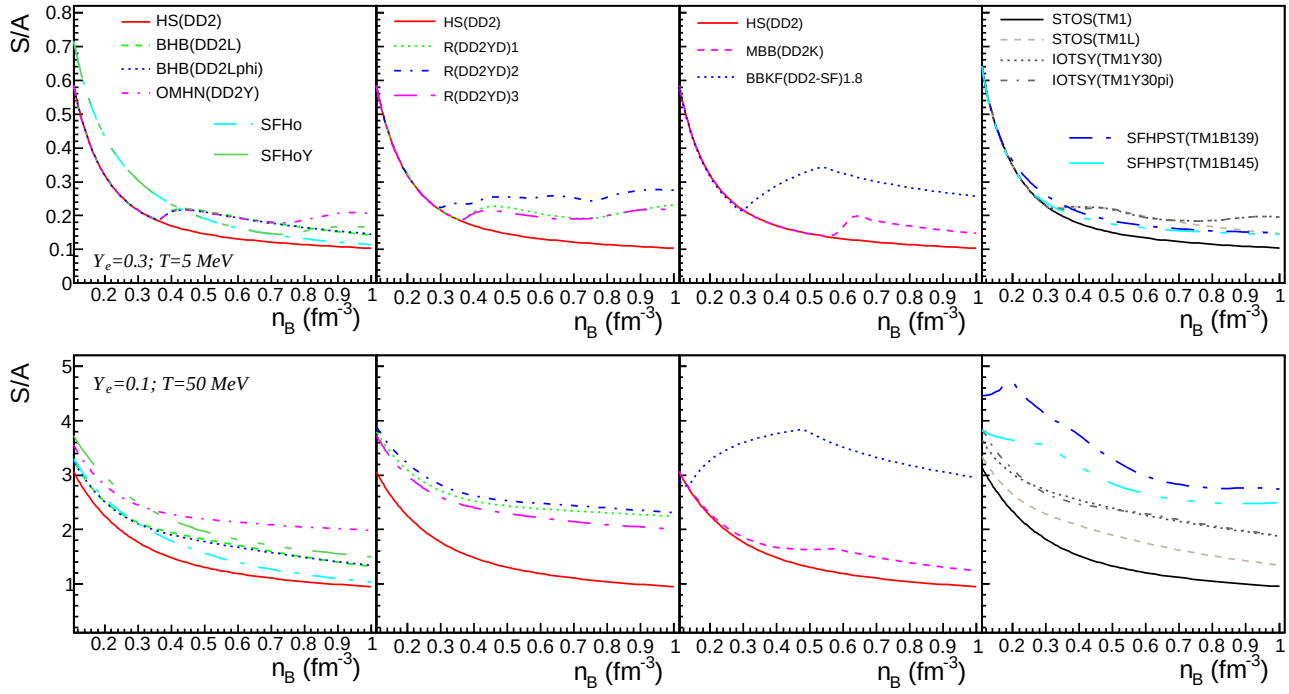

Fig. 19 Baryon (quark) contribution to the entropy per baryon as function of baryon number density for (T=5 MeV, $Y_e = 0.3$) and (T=50 MeV, $Y_e = 0.1$).

various EoS models at different thermodynamic conditions are considered. Γ_S gives an indication about the stiffness of the EoS in all processes occuring at constant entropy.

With the exception of the transition density from clusterized to homogeneous matter $\Gamma_S(n_B)$ of nucleonic EoS models is a smooth function. As discussed in Paper I, nucleonic models manifest a strong dependence of Γ_S on EoS-model and n_B. Fig. 21 shows that at low (high) T, where abundances of heavy baryons and K^- increase steeply (slowly) with baryonic density, EoS models which account for these particles provide $\Gamma_S(n_B)$ with sudden (smooth) changes of slope. The EoS softening produced by hyperons, Δs and K^- leads to $\Gamma_S^{exotic} < \Gamma_S^{nucleonic}$. Predictions of IOTSY(TM1Y30) and IOTSY(TM1Y30pi) are identical or, for the highest T, very similar to those of STOS(TM1L). Also similar are the predictions of the three models that account for $Y\Delta$ introduced in this work. This suggests that modifications in heat capacities, see Fig. 20, are canceled out by modifications in $(\partial \ln P/\partial \ln n_B)|_T$. EoS-models with transitions to quark matter show different features depending on how the transition was dealt with. In the hadron-quark coexistence BBKF-models present a plateau. It stems from the mechanical equilibrium between phases in the Gibbs construction. The high peak at densities slightly exceeding the high density border of phase coexistence is due to the stiff behavior of $P(e)|_T$. At temperatures of the order of a few tens MeV or lower, $\Gamma_S(n_B)$ predicted by SFHPST-models resembles the one of models with heavy baryons and K^-. At temperatures of the order of several tens MeV, $\Gamma_S(n_B)$ of SFHPST(TM1B139) has a high peak at $n_B \approx 1-2n_{sat}$. Quite remarkably, at the highest densities the scattering between different models is limited.

A key quantity in dynamical numerical simulations is the speed of sound v_S. In units of c, the speed of light, it is given by

$$v_S^2 = \frac{dP}{de}|_{S,A,Y_e} = \Gamma_S \frac{P}{e+P} \ . \tag{31}$$

Fig. 22 illustrates its behavior as function of baryon number density within the different EoS models. Different thermodynamic conditions, indicated in the figures, are considered. The three nucleonic models show a strong increase of v_S with n_B and limited sensitivities to the other thermodynamic variables, T and Y_Q. The behavior of $v_S(n_B)$ in DD2 and TM1 differs qualitatively from the one in SFHo: while in DD2 and TM1 the increase gets attenuated at $n \approx 4n_{sat}$, no such effect is seen for SFHo. This situation is attributable to the mixed coupling terms in the latter model. At high densities DD2 provides for the speed of sound a value almost twice larger than the one provided by the softer TM1 model. The CDFT formulation prevents violation of causality. In all circumstances models allowing for hyperons, Δs, π and K^- provide smaller $v_S(n_B)$-values than their nucleonic counterparts. As it was the case with previously considered quantities, sudden modifications in abundances of exotic species are translated into sudden modifications of the

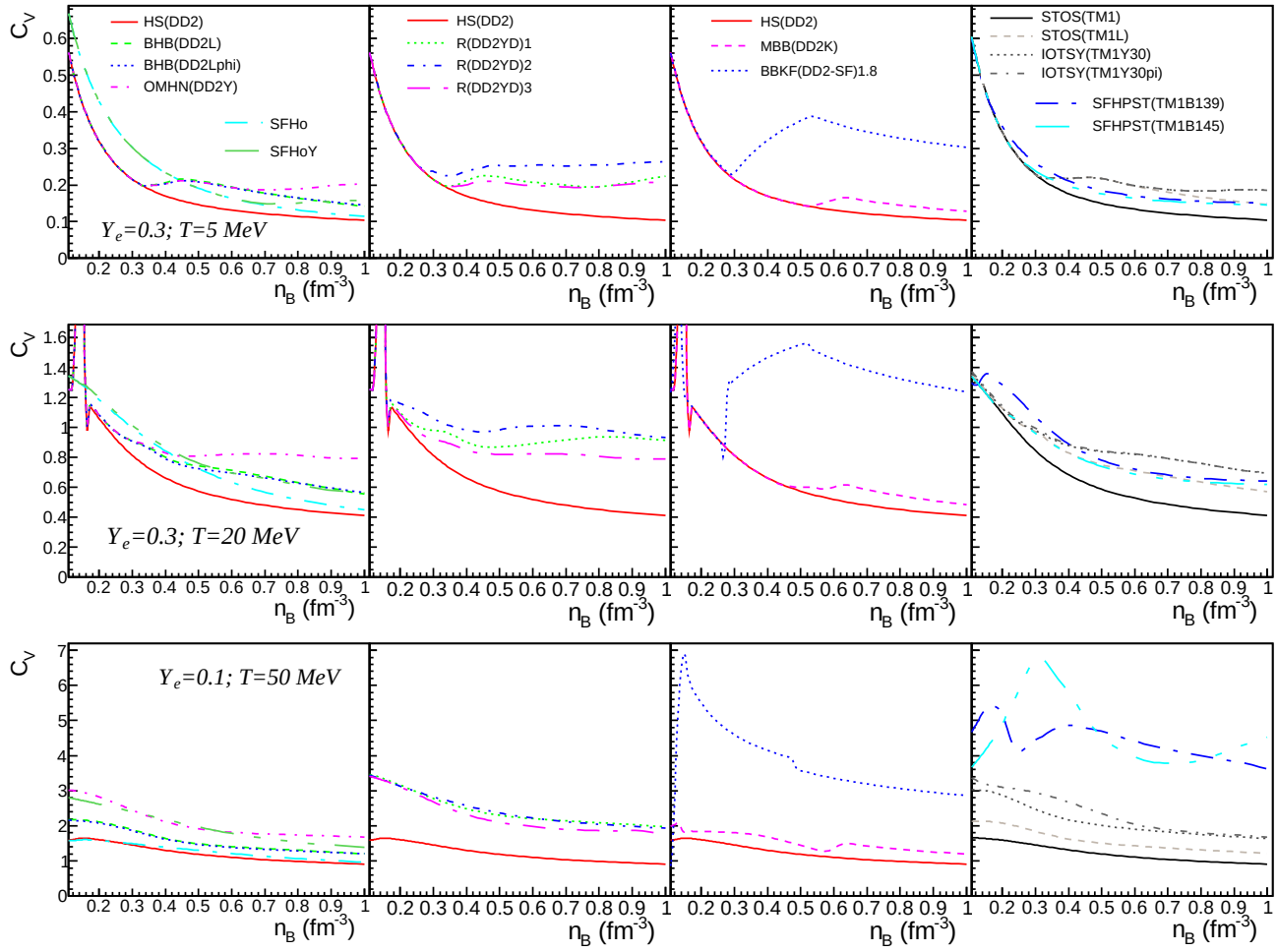

Fig. 20 Specific heat at constant volume, C_V, as function of baryon number density for baryon (quark) matter for (T=5 MeV, $Y_e = 0.3$), (T=20 MeV, $Y_e = 0.3$) and (T=50 MeV, $Y_e = 0.1$).

speed of sound. The T-dependence of v_S remains small as in the considered cases hyperons, Δs, π and K^- are subdominant. As for Γ_S to which v_S is related, chemical equilibrium among hadron and quark phases in BBKF-models leads to vanishing values of the speed of sound. Moreover, in the pure quark phase, BBKF predicts that v_S decreases with n_B. The only other case in Fig. 22 where such a behavior is obtained corresponds to SFHPST(TM1B139) and SFHPST(TM1B145) at the highest considered temperature. Detailed investigation in [29] probes that the same holds true if, instead of constant-T curves, one considers constant S/A-curves. We nevertheless stress that also the nucleonic EoS SRO(SkAPR) [3] provides for the squared speed of sound decreasing evolution with n_B [45]; this means that one should not a priori consider such a behavior as a signature of quark matter. Predictions of IOTSY(TM1Y30) and IOTSY(TM1Y30pi) are identical or very close to those of STOS(TM1L). A very small dispersion is obtained also among the predictions of the three models with hyperons and Δs.

7 Conclusions

Within CDFT we have constructed three general purpose EoS models with hyperons and Δ-resonances ready to use in astrophysical simulations and made them available on the CompOSE repository (`https://compose.obspm.fr/`); to our knowledge these are the first publicly available 3D EoS databases which account for the Δ-quadruplet. The domains of temperature, 0.1 MeV $\leq T \leq$ 100 MeV, baryonic particle number density, 10^{-12} fm$^{-3} \leq n_B \leq 1.1$ fm^{-3} and charge fraction $0.01 \leq Y_Q \leq 0.6$ for which data are provided make them suitable for studies of CCSN and BNS. Also available are databases corresponding to purely baryonic matter, which may be used for heavy ion collision studies. Our models have been built such as to comply with experimental data from nuclear and hyper-nuclear physics; ab initio calculations of neutron matter; astrophysical observations of cold compact stars and - at the same time - partially account for uncertainties related to the population of Δs.

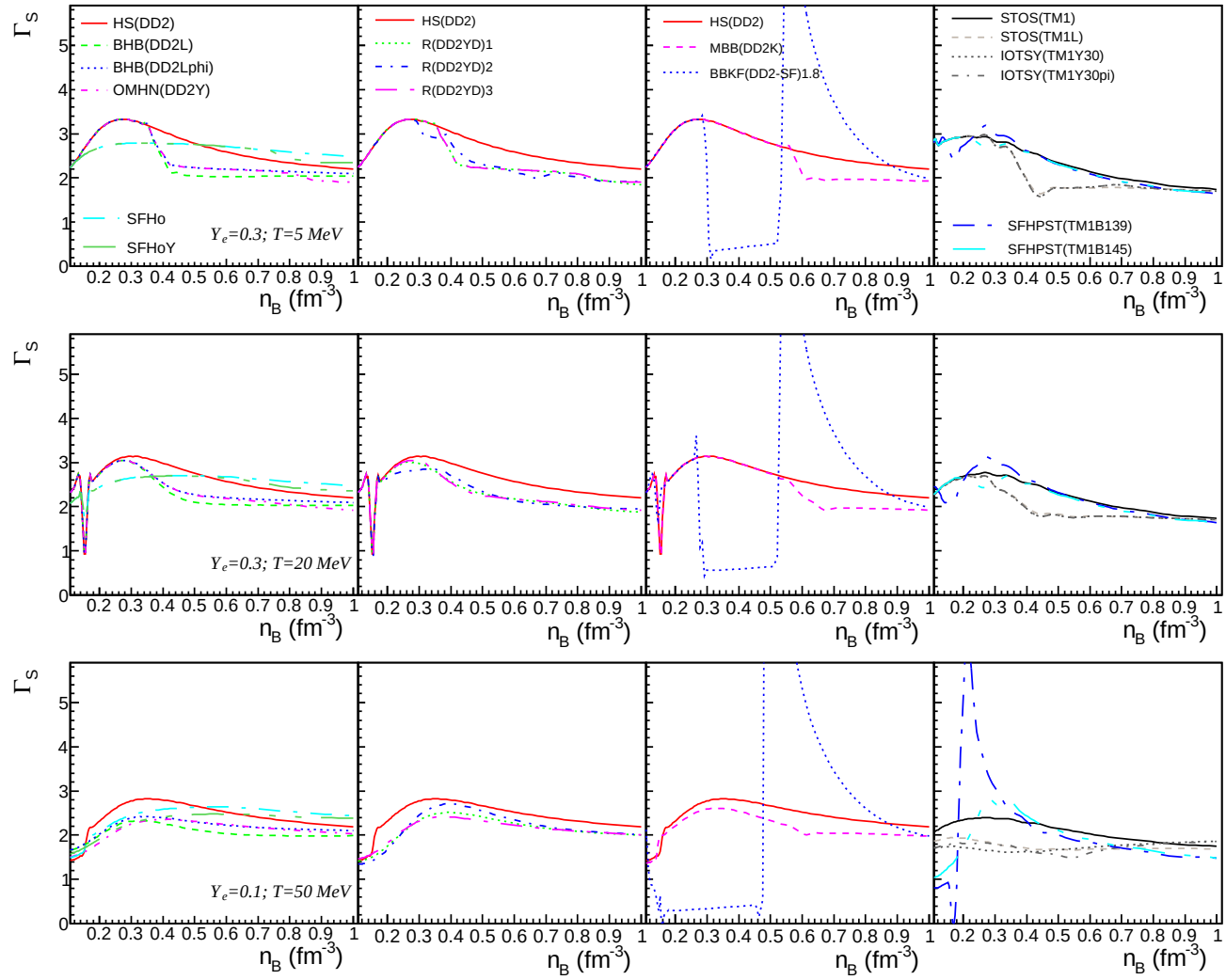

Fig. 21 Γ_S, eq. (30), as function of baryon number density for (T=5 MeV, $Y_e = 0.3$), (T=20 MeV, $Y_e = 0.3$) and (T=50 MeV, $Y_e = 0.1$). Results corresponding to stellar matter, as predicted by various EoS models.

As previously discussed in [44], for certain combinations of coupling constants of the Δ to mesonic fields, the nucleation of Δs may result in thermodynamic instabilities or limit the validity domain of the model by preventing the baryonic number density to exceed values of the order of $2-3n_{sat}$. The latter issue arises because the Dirac effective mass of nucleons vanishes. The present work complements the study performed in [44], and which focuses on cold β-equilibrated matter and persistence of Δ-driven instabilities at finite-T, by considering cold Δ-admixed nuclear matter with extreme values of charge fraction $Y_Q = 0.01$ and 0.5. Present results show that the parameter space which allows for instabilities gets wider as Y_Q diminishes and that, for matter with $Y_Q = 0.5$, purely baryonic and stellar matter exhibit instabilities for the same values of $(x_{\sigma\Delta}, x_{\omega\Delta})$. Both findings are in contrast with the phenomenology of dilute nuclear matter and understandable considering the Δ's abundances.

We have then reviewed the general purpose EoS models with exotic d.o.f. presently available on CompOSE. The information provided for each model includes the nucleonic effective interaction together with the values of the nuclear matter parameters; the exotic d.o.f.; for CDFT models, information on various mesonic fields and values of the hyperon and Δ well depth potentials in symmetric saturated matter on which some meson coupling constants have been tuned; properties of cold β-equilibrated NS and compliance with constraints from compact star observations.

The role of hyperons, Δs, pions, kaons and quarks as well as the consequences of the way in which the hadron-quark phase transition was dealt with have been investigated by analyzing the thermal properties for a number of models; wide ranges of baryonic number density $n_{sat} \lesssim n_B \leq 1$ fm^{-3},

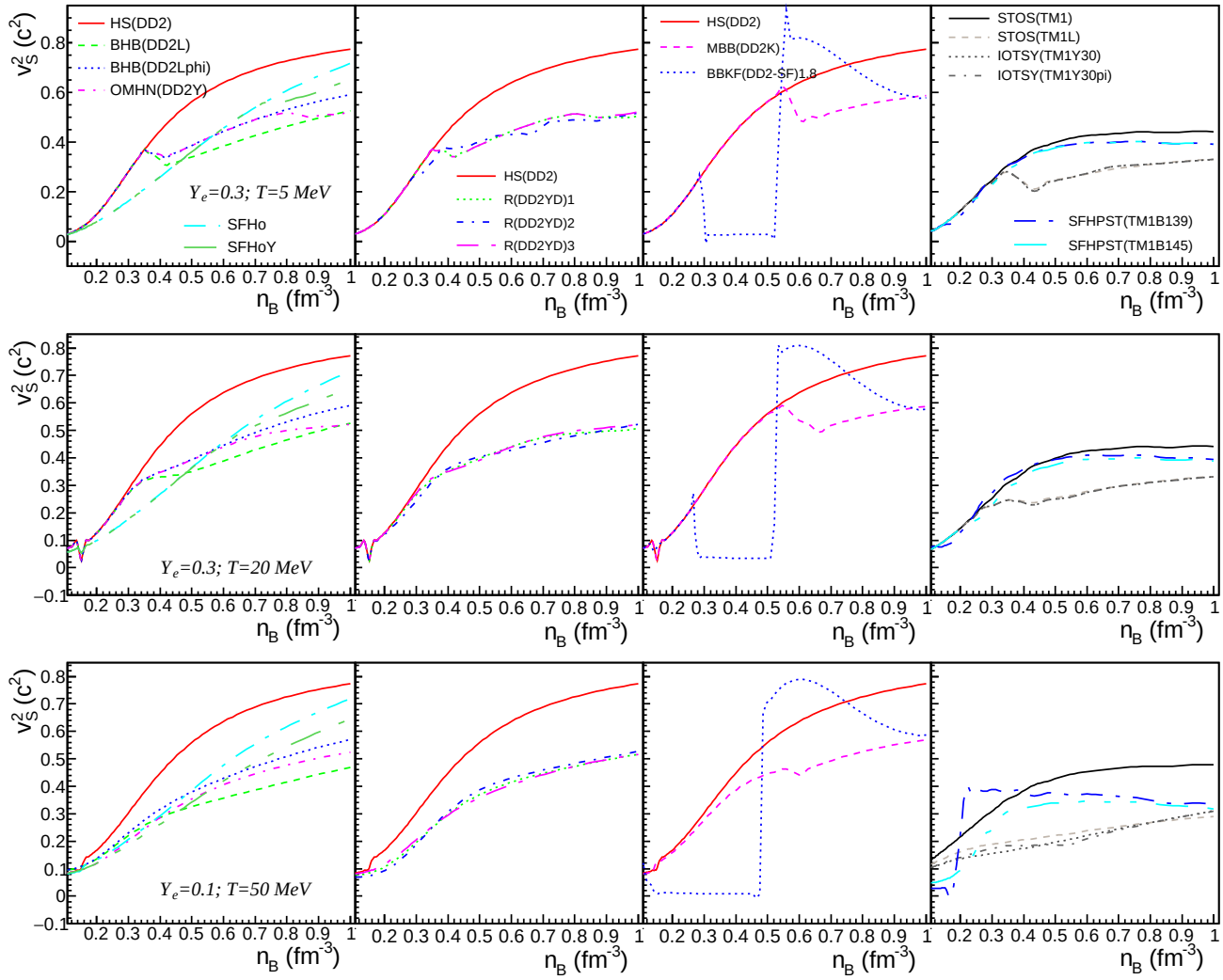

Fig. 22 Speed of sound squared, eq. (31), as function of baryon number density in stellar matter for various EoS models. The considered thermodynamic conditions are: (T=5 MeV, $Y_e = 0.3$), (T=20 MeV, $Y_e = 0.3$) and (T=50 MeV, $Y_e = 0.1$).

temperature 5 MeV $\leq T \leq$ 50 MeV have been considered for charge franctions $Y_Q = 0.1$ and 0.3. In agreement with previous studies we show that extra d.o.f. modify the values of baryon and charge chemical potentials and the modification depends upon the employed nucleonic effective interaction; for fixed values of T, Y_Q and n_B the entropy per baryon increases with the number of species; the behavior of $C_V(n_B)$ replicates the one of $S/A(n_B)$; EoS softening upon nucleation of exotica results in decreased values of the speed of sound; quark matter is characterized by v_S^2 decreasing with n_B. Other results concern the thermal energy density and pressure and the thermal index. Specifically we show that exotic d.o.f. result in thermal energy densities enhanced with respect to what is obtained in purely nucleonic matter; a strongly oscillatory behavior of the thermal pressure and thermal index and, under specific conditions, negative values of p_{th} and $\Gamma_{th;tot}$. The latter feature suggests that the use of the Γ-law for supplementing cold EoS with thermal components is even less advisable for exotic matter than for nucleonic matter. Last but not least we have shown that the way in which the transition from hadronic to quark matter is dealt with impacts on a series of quantities like p_{th}, Γ_{th}, μ_B, Γ_S, v_S^2. BBKF-models show - in the phase coexistence domain - plateaus for all the above listed quantities while no such behavior is obtained in the case of SFHPST-models.

Data Availability Statement his manuscript has no associated data or the data will not be deposited.

[Authors' comment: This manuscript has no associated data as that all data are already available on the CompOSE site `https://compose.obspm.fr/`].

Acknowledgements The author gratefully acknowledges discussions with M. Oertel, C. Providencia and A. Sedrakian. Support from a grant of the Ministry of Research, Innovation and Digitization, CNCS/CCCDI – UEFISCDI, Project No. PN-III-P4-ID-PCE-2020-0293 is also ac-

Table 4 Domains of temperature, baryonic number density and charge fraction covered by the six R(DD2YDelta) EoS tables proposed in this work and the corresponding numbers of mash points.

	T [MeV]	n_B [fm^{-3}]	Y_Q
Number of points	76	302	60
Minimum	0.1	10^{-12}	0.01
Maximum	100	1.1	0.60

knowledged. This work has been partially funded by the European COST Action CA16214 PHAROS "The multi-messenger physics and astrophysics of neutron stars".

Appendix A
See Table 4.

References

1. H.T. Janka, K. Langanke, A. Marek, G. Martinez-Pinedo, B. Mueller, Phys.Rep. **442**(1), 38 (2007). DOI 10.1016/j.physrep.2007.02.002. The Hans Bethe Centennial Volume 1906-2006
2. A. Mezzacappa, E.J. Lentz, S.W. Bruenn, W.R. Hix, O.E.B. Messer, E. Endeve, J.M. Blondin, J.A. Harris, P. Marronetti, K.N. Yakunin, E.J. Lingerfelt, arXiv e-prints arXiv:1507.05680 (2015)
3. A.S. Schneider, L.F. Roberts, C.D. Ott, Phys. Rev. C **96**, 065802 (2017). DOI 10.1103/PhysRevC.96.065802
4. E.P. O'Connor, S.M. Couch, Ap.J. **865**(2), 81 (2018). DOI 10.3847/1538-4357/aadcf7
5. A. Burrows, D. Radice, D. Vartanyan, H. Nagakura, M.A. Skinner, J.C. Dolence, Mon. Not. Roy. Astron. Soc. **491**(2), 2715 (2020). DOI 10.1093/mnras/stz3223
6. M. Shibata, K. Taniguchi, Living Rev. Rel. **14**, 6 (2011). DOI 10.12942/lrr-2011-6
7. S. Rosswog, Int. J. Mod. Phys. D **24**, 1530012 (2015). DOI 10.1142/S0218271815300128
8. L. Baiotti, L. Rezzolla, Rep. Prog. Phys. **80**(9), 096901 (2017). DOI 10.1088/1361-6633/aa67bb
9. A. Endrizzi, D. Logoteta, B. Giacomazzo, I. Bombaci, W. Kastaun, R. Ciolfi, Phys. Rev. D **98**, 043015 (2018). DOI 10.1103/PhysRevD.98.043015
10. M. Ruiz, A. Tsokaros, S.L. Shapiro, Phys. Rev. D **101**(6), 064042 (2020). DOI 10.1103/PhysRevD.101.064042
11. A. Prakash, D. Radice, D. Logoteta, A. Perego, V. Nedora, I. Bombaci, R. Kashyap, S. Bernuzzi, A. Endrizzi, Phys. Rev. D **104**, 083029 (2021). DOI 10.1103/PhysRevD.104.083029
12. E.R. Most, A. Motornenko, J. Steinheimer, V. Dexheimer, M. Hanauske, L. Rezzolla, H. Stoecker, arXiv e-prints arXiv:2201.13150 (2022)
13. J.A. Pons, S. Reddy, M. Prakash, J.M. Lattimer, J.A. Miralles, ApJ **513**(2), 780 (1999). DOI 10.1086/306889
14. A. Pascal, J. Novak, M. Oertel, Mon. Not. Roy. Astron. Soc. **511**(1), 356 (2022). DOI 10.1093/mnras/stac016
15. K. Sumiyoshi, S. Yamada, H. Suzuki, ApJ **667**(1), 382 (2007). DOI 10.1086/520876
16. T. Fischer, S. Whitehouse, A. Mezzacappa, F.K. Thielemann, M. Liebendorfer, Astron. Astrophys. **499**, 1 (2009). DOI 10.1051/0004-6361/200811055
17. E. O'Connor, C.D. Ott, Astrophys. J. **730**, 70 (2011). DOI 10.1088/0004-637X/730/2/70
18. M. Hempel, T. Fischer, J. Schaffner-Bielich, M. Liebendörfer, Ap. J. **748**, 70 (2012). DOI 10.1088/0004-637X/748/1/70
19. Y. Sekiguchi, K. Kiuchi, K. Kyutoku, M. Shibata, Phys. Rev. Lett. **107**, 211101 (2011). DOI 10.1103/PhysRevLett.107.211101
20. D. Radice, S. Bernuzzi, W. Del Pozzo, L.F. Roberts, C.D. Ott, Astrophys. J. Lett. **842**(2), L10 (2017). DOI 10.3847/2041-8213/aa775f
21. A. Bauswein, N.U.F. Bastian, D.B. Blaschke, K. Chatziioannou, J.A. Clark, T. Fischer, M. Oertel, Phys. Rev. Lett. **122**, 061102 (2019). DOI 10.1103/PhysRevLett.122.061102
22. S. Blacker, N.U.F. Bastian, A. Bauswein, D.B. Blaschke, T. Fischer, M. Oertel, T. Soultanis, S. Typel, Phys. Rev. D **102**(12), 123023 (2020). DOI 10.1103/PhysRevD.102.123023
23. E.R. Most, L.J. Papenfort, V. Dexheimer, M. Hanauske, S. Schramm, H. Stöcker, L. Rezzolla, Phys. Rev. Lett. **122**, 061101 (2019). DOI 10.1103/PhysRevLett.122.061101
24. L.R. Weih, M. Hanauske, L. Rezzolla, Phys. Rev. Lett. **124**, 171103 (2020). DOI 10.1103/PhysRevLett.124.171103
25. I. Sagert, T. Fischer, M. Hempel, G. Pagliara, J. Schaffner-Bielich, A. Mezzacappa, F.K. Thielemann, M. Liebendörfer, Phys. Rev. Lett. **102**, 081101 (2009). DOI 10.1103/PhysRevLett.102.081101
26. S. Zha, E.P. O'Connor, M. Chu, L.M. Lin, S.M. Couch, Phys. Rev. Lett. **125**, 051102 (2020). DOI 10.1103/PhysRevLett.125.051102
27. Z. Lin, S. Zha, E.P. O'Connor, A.W. Steiner, arXiv e-prints arXiv: 2203.05141 (2022)
28. B. Peres, M. Oertel, J. Novak, Phys. Rev. D **87**(4), 043006 (2013). DOI 10.1103/PhysRevD.87.043006
29. M.A. Aloy, J.M. Ibáñez, N. Sanchis-Gual, M. Obergaulinger, J.A. Font, S. Serna, A. Marquina, Mon. Not. Roy. Astron. Soc. **484**, 4980 (2019). DOI 10.1093/mnras/stz293
30. J.M. Lattimer, D.F. Swesty, Nucl. Phys. A **535**(2), 331 (1991). DOI 10.1016/0375-9474(91)90452-C
31. H. Shen, H. Toki, K. Oyamatsu, K. Sumiyoshi, Progress of Theoretical Physics **100**(5), 1013 (1998). DOI 10.1143/PTP.100.1013
32. H. Shen, H. Toki, K. Oyamatsu, K. Sumiyoshi, Nuclear Physics A **637**(3), 435 (1998). DOI https://doi.org/10.1016/S0375-9474(98)00236-X
33. M. Oertel, M. Hempel, T. Klähn, S. Typel, Rev. Mod. Phys. **89**, 015007 (2017). DOI 10.1103/RevModPhys.89.015007
34. G. Burgio, H.J. Schulze, I. Vidaña, J.B. Wei, Progress in Particle and Nuclear Physics **120**, 103879 (2021). DOI https://doi.org/10.1016/j.ppnp.2021.103879
35. M. Oertel, A.F. Fantina, J. Novak, Phys. Rev. C **85**, 055806 (2012). DOI 10.1103/PhysRevC.85.055806
36. M. Oertel, F. Gulminelli, C. Providência, A.R. Raduta, Eur. Phys. J. A **52**(3), 50 (2016). DOI 10.1140/epja/i2016-16050-1
37. G. Malfatti, M.G. Orsaria, G.A. Contrera, F. Weber, I.F. Ranea-Sandoval, Phys. Rev. C **100**, 015803 (2019). DOI 10.1103/PhysRevC.100.015803
38. A.R. Raduta, M. Oertel, A. Sedrakian, Mon. Not. Roy. Astron. Soc. **499**(1), 914 (2020). DOI 10.1093/mnras/staa2491
39. S. Khadkikar, A.R. Raduta, M. Oertel, A. Sedrakian, Phys. Rev. C **103**(5), 055811 (2021). DOI 10.1103/PhysRevC.103.055811
40. J.B. Wei, G.F. Burgio, A.R. Raduta, H.J. Schulze, Phys. Rev. C **104**, 065806 (2021). DOI 10.1103/PhysRevC.104.065806
41. A. Sedrakian, A. Harutyunyan, arXiv e-prints (2022)
42. S. Typel, M. Oertel, T. Klaehn, Phys. Part. Nucl. **46**(4), 633 (2015). DOI 10.1134/S1063779615040061
43. S. Typel, et al., arXiv e-prints (2022)
44. A.R. Raduta, Phys. Lett. B **814**, 136070 (2021). DOI 10.1016/j.physletb.2021.136070
45. A.R. Raduta, F. Nacu, M. Oertel, Eur. Phys. J. A **57**(12), 329 (2021). DOI 10.1140/epja/s10050-021-00628-z
46. P.B. Demorest, T. Pennucci, S.M. Ransom, M.S.E. Roberts, J.W.T. Hessels, Nature **467**(7319), 1081 (2010). DOI 10.1038/nature09466

47. J. Antoniadis, P.C.C. Freire, N. Wex, T.M. Tauris, R.S. Lynch, M.H. van Kerkwijk, M. Kramer, C. Bassa, V.S. Dhillon, T. Driebe, J.W.T. Hessels, V.M. Kaspi, V.I. Kondratiev, N. Langer, T.R. Marsh, M.A. McLaughlin, T.T. Pennucci, S.M. Ransom, I.H. Stairs, J. van Leeuwen, J.P.W. Verbiest, D.G. Whelan, Science **340**, 448 (2013). DOI 10.1126/science.1233232
48. Z. Arzoumanian, et al., Astrophys. J. Suppl. **235**(2), 37 (2018). DOI 10.3847/1538-4365/aab5b0
49. H.T. Cromartie, et al., Nature Astron. **4**(1), 72 (2020). DOI 10.1038/s41550-019-0880-2
50. E. Fonseca, H.T. Cromartie, T.T. Pennucci, P.S. Ray, A.Y. Kirichenko, S.M. Ransom, P.B. Demorest, I.H. Stairs, Z. Arzoumanian, L. Guillemot, A. Parthasarathy, M. Kerr, I. Cognard, P.T. Baker, H. Blumer, P.R. Brook, M. DeCesar, T. Dolch, F.A. Dong, E.C. Ferrara, W. Fiore, N. Garver-Daniels, D.C. Good, R. Jennings, M.L. Jones, V.M. Kaspi, M.T. Lam, D.R. Lorimer, J. Luo, A. McEwen, J.W. McKee, M.A. McLaughlin, N. McMann, B.W. Meyers, A. Naidu, C. Ng, D.J. Nice, N. Pol, H.A. Radovan, B. Shapiro-Albert, C.M. Tan, S.P. Tendulkar, J.K. Swiggum, H.M. Wahl, W.W. Zhu, The Astrophysical Journal Letters **915**(1), L12 (2021). DOI 10.3847/2041-8213/ac03b8
51. M.C. Miller, et al., Ap. J. Lett. **887**, L24 (2019). DOI 10.3847/2041-8213/ab50c5
52. T.E. Riley, et al., Ap. J. Lett. **887**, L21 (2019). DOI 10.3847/2041-8213/ab481c
53. M.C. Miller, F.K. Lamb, A.J. Dittmann, S. Bogdanov, Z. Arzoumanian, K.C. Gendreau, S. Guillot, W.C.G. Ho, J.M. Lattimer, M. Loewenstein, S.M. Morsink, P.S. Ray, M.T. Wolff, C.L. Baker, T. Cazeau, S. Manthripragada, C.B. Markwardt, T. Okajima, S. Pollard, I. Cognard, H.T. Cromartie, E. Fonseca, L. Guillemot, M. Kerr, A. Parthasarathy, T.T. Pennucci, S. Ransom, I. Stairs, The Astrophysical Journal Letters **918**(2), L28 (2021). DOI 10.3847/2041-8213/ac089b
54. T.E. Riley, A.L. Watts, P.S. Ray, S. Bogdanov, S. Guillot, S.M. Morsink, A.V. Bilous, Z. Arzoumanian, D. Choudhury, J.S. Deneva, K.C. Gendreau, A.K. Harding, W.C.G. Ho, J.M. Lattimer, M. Loewenstein, R.M. Ludlam, C.B. Markwardt, T. Okajima, C. Prescod-Weinstein, R.A. Remillard, M.T. Wolff, E. Fonseca, H.T. Cromartie, M. Kerr, T.T. Pennucci, A. Parthasarathy, S. Ransom, I. Stairs, L. Guillemot, I. Cognard, The Astrophysical Journal Letters **918**(2), L27 (2021). DOI 10.3847/2041-8213/ac0a81
55. B.P. Abbott, et al., Phys. Rev. Lett. **119**, 161101 (2017). DOI 10.1103/PhysRevLett.119.161101
56. B.P. Abbott, et al., The Astrophysical Journal Letters **848**(2), L12 (2017). DOI 10.3847/2041-8213/aa91c9
57. B. Abbott, et al., Phys. Rev. X **9**(1), 011001 (2019). DOI 10.1103/PhysRevX.9.011001
58. J. Negele, D. Vautherin, Nuclear Physics A **207**(2), 298 (1973). DOI https://doi.org/10.1016/0375-9474(73)90349-7
59. P. Haensel, J.L. Zdunik, J. Dobaczewski, Astronomy and Astrophysics **222**(1-2), 353 (1989)
60. H. Shen, H. Toki, K. Oyamatsu, K. Sumiyoshi, The Astrophysical Journal Supplement Series **197**(2), 20 (2011). DOI 10.1088/0067-0049/197/2/20
61. C. Ishizuka, A. Ohnishi, K. Tsubakihara, K. Sumiyoshi, S. Yamada, Journal of Physics G: Nuclear and Particle Physics **35**(8), 085201 (2008). DOI 10.1088/0954-3899/35/8/085201
62. I. Sagert, T. Fischer, M. Hempel, G. Pagliara, J. Schaffner-Bielich, F.K. Thielemann, M. Liebendörfer, Journal of Physics G: Nuclear and Particle Physics **37**(9), 094064 (2010). DOI 10.1088/0954-3899/37/9/094064
63. T. Fischer, I. Sagert, G. Pagliara, M. Hempel, J. Schaffner-Bielich, T. Rauscher, F.K. Thielemann, R. Kappeli, G. Martinez-Pinedo, M. Liebendorfer, Astrophys. J. Suppl. **194**, 39 (2011). DOI 10.1088/0067-0049/194/2/39
64. M. Hempel, J. Schaffner-Bielich, Nucl. Phys. A **837**, 210 (2010). DOI 10.1016/j.nuclphysa.2010.02.010
65. A.W. Steiner, M. Hempel, T. Fischer, The Astrophysical Journal **774**(1), 17 (2013). DOI 10.1088/0004-637x/774/1/17
66. M. Fortin, M. Oertel, C. Providência, Publ. Astron. Soc. Austral. **35**, 44 (2018). DOI 10.1017/pasa.2018.32
67. S. Banik, M. Hempel, D. Bandyopadhyay, The Astrophysical Journal Supplement Series **214**(2), 22 (2014). DOI 10.1088/0067-0049/214/2/22
68. M. Marques, M. Oertel, M. Hempel, J. Novak, Phys. Rev. C **96**, 045806 (2017). DOI 10.1103/PhysRevC.96.045806
69. T. Malik, S. Banik, D. Bandyopadhyay, The European Physical Journal Special Topics **230**, 561 (2021). DOI 10.1140/epjs/s11734-021-00006-2
70. T. Malik, S. Banik, D. Bandyopadhyay, The Astrophysical Journal **910**(2), 96 (2021). DOI 10.3847/1538-4357/abe860
71. P. Guichon, Physics Letters B **200**(3), 235 (1988). DOI https://doi.org/10.1016/0370-2693(88)90762-9
72. P. Guichon, J. Stone, A. Thomas, Progress in Particle and Nuclear Physics **100**, 262 (2018). DOI https://doi.org/10.1016/j.ppnp.2018.01.008
73. J.R. Stone, V. Dexheimer, P.A.M. Guichon, A.W. Thomas, S. Typel, Mon. Not. Roy. Astron. Soc. **502**(3), 3476 (2021). DOI 10.1093/mnras/staa4006
74. V. Dexheimer, R. Negreiros, S. Schramm, Phys. Rev. C **92**, 012801 (2015). DOI 10.1103/PhysRevC.92.012801
75. V. Dexheimer, Publications of the Astronomical Society of Australia **34** (2017). DOI 10.1017/pasa.2017.61
76. M.A.R. Kaltenborn, N.U.F. Bastian, D.B. Blaschke, Phys. Rev. D **96**, 056024 (2017). DOI 10.1103/PhysRevD.96.056024
77. N.U.F. Bastian, Phys. Rev. D **103**, 023001 (2021). DOI 10.1103/PhysRevD.103.023001
78. Y. Sugahara, H. Toki, Nuclear Physics A **579**(3), 557 (1994). DOI https://doi.org/10.1016/0375-9474(94)90923-7
79. S. Typel, G. Röpke, T. Klähn, D. Blaschke, H.H. Wolter, Phys. Rev. C **81**, 015803 (2010). DOI 10.1103/PhysRevC.81.015803
80. D. Alvarez-Castillo, A. Ayriyan, S. Benic, D. Blaschke, H. Grigorian, S. Typel, Eur. Phys. J. A **52**(3), 69 (2016). DOI 10.1140/epja/i2016-16069-2
81. V. Dexheimer, S. Schramm, The Astrophysical Journal **683**(2), 943 (2008). DOI 10.1086/589735
82. T.A. Rijken, M.M. Nagels, Y. Yamamoto, Progress of Theoretical Physics Supplement **185**, 14 (2010). DOI 10.1143/PTPS.185.14
83. M.M. Nagels, T.A. Rijken, Y. Yamamoto, Phys. Rev. C **99**, 044003 (2019). DOI 10.1103/PhysRevC.99.044003
84. J. Haidenbauer, U.G. Meißner, A. Nogga, Eur. Phys. J. A **56**(3), 91 (2020). DOI 10.1140/epja/s10050-020-00100-4
85. H.J. Schulze, A. Polls, A. Ramos, I. Vidaña, Phys. Rev. C **73**, 058801 (2006). DOI 10.1103/PhysRevC.73.058801
86. G.F. Burgio, H.J. Schulze, A. Li, Phys. Rev. C **83**, 025804 (2011). DOI 10.1103/PhysRevC.83.025804
87. T.A. Rijken, H.J. Schulze, Eur. Phys. J. A **52**(2), 21 (2016). DOI 10.1140/epja/i2016-16021-6
88. Kochankovski, Hristijan, Ramos, Àngels, Vidaña, Isaac, DOI 10.1140/epja/s10050-022-00669-y
89. D.J. Millener, C.B. Dover, A. Gal, Phys. Rev. C **38**, 2700 (1988)
90. M. Fortin, S.S. Avancini, C. Providência, I. Vidaña, Phys. Rev. C **95**, 065803 (2017). DOI 10.1103/PhysRevC.95.065803
91. M. Fortin, A.R. Raduta, S. Avancini, C. Providência, Phys. Rev. D **101**(3), 034017 (2020). DOI 10.1103/PhysRevD.101.034017
92. A. Gal, E.V. Hungerford, D.J. Millener, Rev. Mod. Phys. **88**, 035004 (2016). DOI 10.1103/RevModPhys.88.035004
93. E. Friedman, A. Gal, Physics Letters B **820**, 136555 (2021). DOI https://doi.org/10.1016/j.physletb.2021.136555
94. H. Takahashi, J.K. Ahn, H. Akikawa, S. Aoki, K. Arai, S.Y. Bahk, K.M. Baik, B. Bassalleck, J.H. Chung, M.S. Chung, D.H. Davis, T. Fukuda, K. Hoshino, A. Ichikawa, M. Ieiri,

K. Imai, Y.H. Iwata, Y.S. Iwata, H. Kanda, M. Kaneko, T. Kawai, M. Kawasaki, C.O. Kim, J.Y. Kim, S.J. Kim, S.H. Kim, Y. Kondo, T. Kouketsu, Y.L. Lee, J.W.C. McNabb, M. Mitsuhara, Y. Nagase, C. Nagoshi, K. Nakazawa, H. Noumi, S. Ogawa, H. Okabe, K. Oyama, H.M. Park, I.G. Park, J. Parker, Y.S. Ra, J.T. Rhee, A. Rusek, H. Shibuya, K.S. Sim, P.K. Saha, D. Seki, M. Sekimoto, J.S. Song, T. Takahashi, F. Takeutchi, H. Tanaka, K. Tanida, J. Tojo, H. Torii, S. Torikai, D.N. Tovee, N. Ushida, K. Yamamoto, N. Yasuda, J.T. Yang, C.J. Yoon, C.S. Yoon, M. Yosoi, T. Yoshida, L. Zhu, Phys. Rev. Lett. **87**, 212502 (2001). DOI 10.1103/PhysRevLett.87.212502

95. J.K. Ahn, H. Akikawa, S. Aoki, K. Arai, S.Y. Bahk, K.M. Baik, B. Bassalleck, J.H. Chung, M.S. Chung, D.H. Davis, T. Fukuda, K. Hoshino, A. Ichikawa, M. Ieiri, K. Imai, K. Itonaga, Y.H. Iwata, Y.S. Iwata, H. Kanda, M. Kaneko, T. Kawai, M. Kawasaki, C.O. Kim, J.Y. Kim, S.H. Kim, S.J. Kim, Y. Kondo, T. Kouketsu, H.N. Kyaw, Y.L. Lee, J.W.C. McNabb, A.A. Min, M. Mitsuhara, K. Miwa, K. Nakazawa, Y. Nagase, C. Nagoshi, Y. Nakanishi, H. Noumi, S. Ogawa, H. Okabe, K. Oyama, B.D. Park, H.M. Park, I.G. Park, J. Parker, Y.S. Ra, J.T. Rhee, A. Rusek, A. Sawa, H. Shibuya, K.S. Sim, P.K. Saha, D. Seki, M. Sekimoto, J.S. Song, H. Takahashi, T. Takahashi, F. Takeutchi, H. Tanaka, K. Tanida, K.T. Tint, J. Tojo, H. Torii, S. Torikai, D.N. Tovee, T. Tsunemi, M. Ukai, N. Ushida, T. Wint, K. Yamamoto, N. Yasuda, J.T. Yang, C.J. Yoon, C.S. Yoon, M. Yosoi, T. Yoshida, L. Zhu, Phys. Rev. C **88**, 014003 (2013). DOI 10.1103/PhysRevC.88.014003
96. M. Fortin, A.R. Raduta, S. Avancini, C. Providência, Phys. Rev. D **103**(8), 083004 (2021). DOI 10.1103/PhysRevD.103.083004
97. N.K. Glendenning, Phys. Rev. D **46**, 1274 (1992). DOI 10.1103/PhysRevD.46.1274
98. M. Fortin, C. Providência, A.R. Raduta, F. Gulminelli, J.L. Zdunik, P. Haensel, M. Bejger, Phys. Rev. C **94**, 035804 (2016). DOI 10.1103/PhysRevC.94.035804
99. J. Walecka, Annals of Physics **83**(2), 491 (1974). DOI https://doi.org/10.1016/0003-4916(74)90208-5
100. M. Dutra, O. Lourenço, S.S. Avancini, B.V. Carlson, A. Delfino, D.P. Menezes, C. Providencia, S. Typel, J.R. Stone, Phys. Rev. **C90**(5), 055203 (2014). DOI 10.1103/PhysRevC.90.055203
101. T. Gaitanos, M.D. Toro, S. Typel, V. Baran, C. Fuchs, V. Greco, H. Wolter, Nuclear Physics A **732**, 24 (2004). DOI https://doi.org/10.1016/j.nuclphysa.2003.12.001
102. X. Roca-Maza, X. Viñas, M. Centelles, P. Ring, P. Schuck, Phys. Rev. C **84**, 054309 (2011). DOI 10.1103/PhysRevC.84.054309
103. D.P. Menezes, C. Providência, Phys. Rev. C **70**, 058801 (2004). DOI 10.1103/PhysRevC.70.058801
104. H. Lenske, M. Dhar, T. Gaitanos, X. Cao, Prog. Part. Nucl. Phys. **98**, 119 (2018). DOI 10.1016/j.ppnp.2017.09.001
105. A. Drago, A. Lavagno, G. Pagliara, D. Pigato, Phys. Rev. C **90**, 065809 (2014). DOI 10.1103/PhysRevC.90.065809
106. E. Kolomeitsev, K. Maslov, D. Voskresensky, Nuclear Physics A **961**, 106 (2017). DOI https://doi.org/10.1016/j.nuclphysa.2017.02.004
107. B.J. Cai, F.J. Fattoyev, B.A. Li, W.G. Newton, Phys. Rev. C **92**, 015802 (2015). DOI 10.1103/PhysRevC.92.015802
108. Z.Y. Zhu, A. Li, J.N. Hu, H. Sagawa, Phys. Rev. C **94**, 045803 (2016). DOI 10.1103/PhysRevC.94.045803
109. J.M. Lattimer, M. Prakash, Phys. Rept. **442**, 109 (2007). DOI 10.1016/j.physrep.2007.02.003
110. J.J. Li, A. Sedrakian, F. Weber, Phys. Lett. B **783**, 234 (2018). DOI 10.1016/j.physletb.2018.06.051
111. P. Ribes, A. Ramos, L. Tolos, C. Gonzalez-Boquera, M. Centelles, ApJ **883**, 168 (2019). DOI 10.3847/1538-4357/ab3a93
112. J.J. Li, A. Sedrakian, Astrophys. J. Lett. **874**(2), L22 (2019). DOI 10.3847/2041-8213/ab1090
113. A. Bodek, T. Cai, Eur. Phys. J. C **80**(7), 655 (2020). DOI 10.1140/epjc/s10052-020-8236-8
114. M.D. Cozma, M.B. Tsang, Eur. Phys. J. A **57**(11), 309 (2021). DOI 10.1140/epja/s10050-021-00616-3
115. W. Spinella, A systematic investigation of exotic matter in neutron stars. Ph.D. thesis, Claremont Graduate University/San Diego State University (2017)
116. A. Lavagno, D. Pigato, Physica A **531**, 121595 (2019). DOI 10.1016/j.physa.2019.121595
117. C. Ducoin, P. Chomaz, F. Gulminelli, Nuclear Physics A **771**, 68 (2006). DOI https://doi.org/10.1016/j.nuclphysa.2006.03.005
118. C. Ducoin, P. Chomaz, F. Gulminelli, Nucl. Phys. A **781**, 407 (2007). DOI 10.1016/j.nuclphysa.2006.11.047
119. A. Rios, Nucl. Phys. A **845**, 58 (2010). DOI 10.1016/j.nuclphysa.2010.05.057
120. C. Ducoin, C. Providencia, A.M. Santos, L. Brito, P. Chomaz, Phys. Rev. C **78**, 055801 (2008). DOI 10.1103/PhysRevC.78.055801
121. S. Typel, H.H. Wolter, G. Röpke, D. Blaschke, Eur. Phys. J. A **50**, 17 (2014). DOI 10.1140/epja/i2014-14017-x
122. A. Rios, A. Polls, A. Ramos, H. Müther, Phys. Rev. C **78**, 044314 (2008). DOI 10.1103/PhysRevC.78.044314
123. A. Carbone, A. Polls, A. Rios, Phys. Rev. C **98**(2), 025804 (2018). DOI 10.1103/PhysRevC.98.025804
124. F. Gulminelli, A. Raduta, M. Oertel, Phys. Rev. C **86**, 025805 (2012). DOI 10.1103/PhysRevC.86.025805
125. F. Gulminelli, A. Raduta, M. Oertel, J. Margueron, Phys. Rev. C **87**(5), 055809 (2013). DOI 10.1103/PhysRevC.87.055809
126. M. Oertel, C. Providência, F. Gulminelli, A.R. Raduta, J. Phys. G **42**(7), 075202 (2015). DOI 10.1088/0954-3899/42/7/075202
127. J.R. Torres, F. Gulminelli, D.P. Menezes, Phys. Rev. C **95**(2), 025201 (2017). DOI 10.1103/PhysRevC.95.025201
128. C. Constantinou, B. Muccioli, M. Prakash, J.M. Lattimer, Phys. Rev. C **89**, 065802 (2014). DOI 10.1103/PhysRevC.89.065802
129. C. Constantinou, B. Muccioli, M. Prakash, J.M. Lattimer, Phys. Rev. C **92**, 025801 (2015). DOI 10.1103/PhysRevC.92.025801
130. K. Hotokezaka, K. Kiuchi, K. Kyutoku, T. Muranushi, Y. Sekiguchi, M. Shibata, K. Taniguchi, Phys. Rev. D **88**, 044026 (2013). DOI 10.1103/PhysRevD.88.044026
131. A. Bauswein, H.T. Janka, R. Oechslin, Phys. Rev. D **82**, 084043 (2010). DOI 10.1103/PhysRevD.82.084043
132. G. Camelio, T. Dietrich, M. Marques, S. Rosswog, Phys. Rev. D **100**(12), 123001 (2019). DOI 10.1103/PhysRevD.100.123001